

CANADIAN THESES ON MICROFICHE

I.S.B.N.

THÈSES CANADIENNES SUR MICROFICHE



National Library of Canada
Collections Development Branch

Canadian Theses on
Microfiche Service

Ottawa, Canada
K1A 0N4

Bibliothèque nationale du Canada
Direction du développement des collections

Service des thèses canadiennes
sur microfiche

NOTICE

The quality of this microfiche is heavily dependent upon the quality of the original thesis submitted for microfilming. Every effort has been made to ensure the highest quality of reproduction possible.

If pages are missing, contact the university which granted the degree.

Some pages may have indistinct print especially if the original pages were typed with a poor typewriter ribbon or if the university sent us a poor photocopy.

Previously copyrighted materials (journal articles, published tests, etc.) are not filmed.

Reproduction in full or in part of this film is governed by the Canadian Copyright Act, R.S.C. 1970, c. C-30. Please read the authorization forms which accompany this thesis.

**THIS DISSERTATION
HAS BEEN MICROFILMED
EXACTLY AS RECEIVED**

AVIS

La qualité de cette microfiche dépend grandement de la qualité de la thèse soumise au microfilmage. Nous avons tout fait pour assurer une qualité supérieure de reproduction.

S'il manque des pages, veuillez communiquer avec l'université qui a conféré le grade.

La qualité d'impression de certaines pages peut laisser à désirer, surtout si les pages originales ont été dactylographiées à l'aide d'un ruban usé ou si l'université nous a fait parvenir une photocopie de mauvaise qualité.

Les documents qui font déjà l'objet d'un droit d'auteur (articles de revue, examens publiés, etc.) ne sont pas microfilmés.

La reproduction, même partielle, de ce microfilm est soumise à la Loi canadienne sur le droit d'auteur, SRC 1970, c. C-30. Veuillez prendre connaissance des formules d'autorisation qui accompagnent cette thèse.

**LA THÈSE A ÉTÉ
MICROFILMÉE TELLE QUE
NOUS L'AVONS REÇUE**



National Library of Canada

Bibliothèque nationale du Canada

Canadian Theses Division / Division des thèses canadiennes

Ottawa, Canada
K1A 0N4

63894

0-315-15985-5

PERMISSION TO MICROFILM — AUTORISATION DE MICROFILMER

• Please print or type — Écrire en lettres moulées ou dactylographier

Full Name of Author — Nom complet de l'auteur

KENNETH RICHARD FYFE

Date of Birth — Date de naissance

23 FEB 58

Country of Birth — Lieu de naissance

CANADA

Permanent Address — Résidence fixe

RR #1
FORT SASKATCHEWAN
ALBERTA T8L 2N7

Title of Thesis — Titre de la thèse

PRACTICAL IMPLEMENTATION OF MODAL ANALYSIS

University — Université

UNIVERSITY OF ALBERTA

Degree for which thesis was presented — Grade pour lequel cette thèse fut présentée

M.Sc.

Year this degree conferred — Année d'obtention de ce grade

1983

Name of Supervisor — Nom du directeur de thèse

Dr M.G. FAULKNER

Permission is hereby granted to the NATIONAL LIBRARY OF CANADA to microfilm this thesis and to lend or sell copies of the film.

The author reserves other publication rights, and neither the thesis nor extensive extracts from it may be printed or otherwise reproduced without the author's written permission.

L'autorisation est, par la présente, accordée à la BIBLIOTHÈQUE NATIONALE DU CANADA de microfilmer cette thèse et de prêter ou de vendre des exemplaires du film.

L'auteur se réserve les autres droits de publication; ni la thèse ni de longs extraits de celle-ci ne doivent être imprimés ou autrement reproduits sans l'autorisation écrite de l'auteur.

Date

Dec 15, 1982

Signature

Ken Fyfe

THE UNIVERSITY OF ALBERTA

PRACTICAL IMPLEMENTATION OF MODAL ANALYSIS

by

C
KEN FYFE

A THESIS

SUBMITTED TO THE FACULTY OF GRADUATE STUDIES AND RESEARCH
IN PARTIAL FULFILMENT OF THE REQUIREMENTS FOR THE DEGREE
OF MASTER OF SCIENCE

DEPARTMENT OF MECHANICAL ENGINEERING

EDMONTON, ALBERTA

SPRING 1983

THE UNIVERSITY OF ALBERTA

RELEASE FORM

NAME OF AUTHOR KEN FYFE
TITLE OF THESIS PRACTICAL IMPLEMENTATION OF MODAL
 ANALYSIS
DEGREE FOR WHICH THESIS WAS PRESENTED MASTER OF SCIENCE
YEAR THIS DEGREE GRANTED SPRING 1983

Permission is hereby granted to THE UNIVERSITY OF ALBERTA LIBRARY to reproduce single copies of this thesis and to lend or sell such copies for private, scholarly or scientific research purposes only.

The author reserves other publication rights, and neither the thesis nor extensive extracts from it may be printed or otherwise reproduced without the author's written permission.

(SIGNED) .. *Ken Fyfe* ..

PERMANENT ADDRESS:

.. RR#1 ..
.. FORT SASKATCHEWAN ..
.. ALBERTA .. T8L 2N7 .. }

DATED .. *Dec 15* .. 19 *82*

THE UNIVERSITY OF ALBERTA
FACULTY OF GRADUATE STUDIES AND RESEARCH

The undersigned certify that they have read, and recommend to the Faculty of Graduate Studies and Research, for acceptance, a thesis entitled PRACTICAL IMPLEMENTATION OF MODAL ANALYSIS submitted by KEN FYFE in partial fulfilment of the requirements for the degree of MASTER OF SCIENCE.

Gay Faulkner

Supervisor

R. E. Rink

W. Kennedy

Date..... December 13, 1982

Dedicated to my wife and parents

ABSTRACT

Modal Analysis is becoming an integral part in the design phase and trouble-shooting aspects of noise and vibration related problems. Low cost digital hardware and increasingly efficient software have facilitated the widespread use of this technique.

A study is made into the implementation of the impulse loading method for the purpose of determining the modal parameters of a structure using transfer function analysis.

From this study, a practical modal analysis approach is outlined that is designed to be used without the aid of specialized modal analysis units. Details of this procedure include: aspects of data acquisition, windowing in the time and frequency domains, curve fitting and the use of curve fit values to estimate the modal parameters in question.

Tests were performed on a continuous free-free beam to verify the technique by comparing the results with those predicted from theory. The technique was then applied to a practical engineering problem: dynamic analysis of an air compressor and its inertial base.

Acknowledgements

The Author wishes to thank Dr. M.G. Faulkner for his encouragement, guidance and invaluable advice in seeing this thesis to its completion.

Thanks are also extended to the Department of Mechanical Engineering (University of Alberta) and the Natural Sciences and Engineering Research Council of Canada (NSERC grant A7514) for funding throughout the project.

Table of Contents

Chapter	Page
1. INTRODUCTION	1
1.1 F.E.M. and Modal Testing	1
1.2 Practical Modal Analysis	2
1.3 Research Outline	4
2. THEORETICAL CONSIDERATIONS	6
2.1 Transfer Functions in the Laplace Domain	6
2.2 Residue Matrix Properties	8
2.3 Frequency Response Function	10
2.4 Discrete Fourier Transform	12
2.5 Windowing	14
3. IDENTIFICATION OF MODAL PARAMETERS	20
3.1 Levy Curve Fit	22
3.2 A True MDOF Curve Fit	26
3.3 Mode Shape Determination	33
4. PRACTICAL CONSIDERATIONS	37
4.1 Choice of Loading	37
4.2 Selection of Transducers and Calibration	39
4.3 Test Point Determination	40
4.4 Equipment and Testing	41
4.5 Digitization of Signals	44
4.6 Coherence	44
5. TEST RESULTS	49
5.1 Free-Free Beam	49
5.2 Compressor and Base	54
6. CONCLUSIONS	68

REFERENCES70
APPENDIX A - LEVY PROGRAM72
APPENDIX B - NON-SIMULTANEOUS SAMPLING76

List of Tables

Table		Page
5.1	Experimental vs. Theoretical Resonant Frequencies for the Free-Free Beam	53
5.2	Normalized Modal Vectors for the Free-Free Beam	53
5.3	Resonant Frequencies and Damping Ratios of the Compressor System	63

List of Figures

Figure	Page
2.1 Forcing Signal	17
2.2 Response Signal	17
3.1 MDOF Transfer Function	21
3.2 Levy Curve Fit	30
3.3 Levy Curve Fit and Additional Terms	30
3.4 True Least-Squares Curve Fit	31
4.1 Equipment used to Record Data	42
4.2 Equipment used to Digitize Signals	42
4.3 Coherence of Tape Recorded Signal	48
5.1 Mode Shape of the 167 Hz Mode	55
5.2 Mode Shape of the 462 Hz Mode	55
5.3 Mode Shape of the 906 Hz Mode	55
5.4 Six Rigid Body Modes	57
5.5 Test Points on Compressor System	57
5.6 Transfer Function in X-Y Plane	60
5.7 Transfer Function in Y-Z Plane	60
5.8 Transfer Function in X-Z Plane	61
5.9 Mode Shape of the 6.51 Hz Mode	65
5.10 Mode Shape of the 6.30 Hz Mode	65
5.11 Mode Shape of the 5.44 Hz Mode	66
5.12 Mode Shape of the 4.72 Hz Mode	66
5.13 Mode Shape of the 3.22 Hz Mode	67
5.14 Mode Shape of the 3.06 Hz Mode	67

Nomenclature

a_k	component of residue matrix
A_0, A_1, \dots	coefficients of numerator function, $N(\omega)$
$[A_k]$	residue matrix
B_1, B_2, \dots	coefficients of denominator function, $D(\omega)$
$[B(s)]$	system matrix
C	lower residual term of analytical curve fit function
$[C]$	damping matrix
D	upper residual term of analytical curve fit function
$D(\omega)$	denominator function of Levy expansion
f	frequency
$g(t)$	time domain signal
$G(f)$	Fourier transform of $g(t)$
$[H(s)]$	transfer matrix
$[I]$	identity matrix
k	pertaining to the k th mode
$[K]$	stiffness matrix
$[M]$	mass matrix
n	number of modes
N	number of time sample points
$N(\omega)$	numerator function of Levy expansion
p_k	system pole
s	complex variable
Δt	sampling interval
T	length of time record
$\{u_k\}$	modal vector

$w(t)$	windowing function
$\{x(t)\}$	displacement vector
a_k	complex constant
β	amount of damping in exponential window
$\gamma^2(f)$	coherence function
$e(\omega)$	error function
ζ	damping ratio
α	damping coefficient
ω	damped circular frequency
*	denotes complex conjugate

1. INTRODUCTION

1.1 F.E.M. and Modal Testing

Exact, closed form solutions describing the dynamic behavior of a body exist for but a few simple homogeneous configurations. For more complex structures, it is necessary to use alternate methods to determine their vibrational characteristics. Commonly employed procedures are finite element analysis and modal testing methods.

In finite element analysis, the structure is divided into a finite number of discrete elements. The equations of motion of the individual elements along with the constraining boundary conditions, together describe the overall motion of the body. Once this mathematical model has been formed, it can be used very effectively to study both the static and dynamic behavior of the body due to any number of different loading conditions. The effects of changes in design and material selection can at once be determined, whereas actual prototype testing would be a much slower and more expensive route to choose.

Designing using the finite element method, does have its problems however. They include; the large computer programs and memory space required to model the structure adequately and the often large discrepancies between predicted and actual test results. Direct dynamic testing, then is necessary to determine the validity of any computer modelling that is carried out.

Dynamic or modal testing is normally of one of two types; normal mode or transfer function methods. In normal mode testing, resonant modes are excited one at a time (using shaker tables) and the natural frequencies, damping and mode shapes can be determined. This process however, is difficult to use when two adjacent modes are close together because of the problem of exciting only one mode at a time, especially if the damping is appreciable. Another problem with this method is its limited versatility. Field testing is very impractical because of the large amount of equipment to set up, and the analysis of large structures is limited by the size and number of shaker tables available.

The transfer function method is superior to the normal mode method, in that all of the dominant modes can be measured simultaneously. As well a large variety of single unit exciting methods can be employed to force the structure which helps keep equipment and time requirements to a minimum. By using the Fourier transform to determine the transfer function between various points on the test structure, and curve fitting these experimental transfer functions to a standard form, it is possible to quickly determine the vibrational properties of the structure.

1.2 Practical Modal Analysis

Transfer function test signals are usually digitized right on location using dual channel FFT analyzers. For the purpose of this study, however, it was deemed more useful to

record raw field data on a portable multichannel, FM tape recorder. The main reason for choosing this route was that many applications of the type of analysis require the taking of data in dirty or hazardous environments (e.g. chemical refineries). In this way, test data could be quickly stored on tape and later played back for analysis. A second and perhaps as important a reason as the first, is that it allows flexibility in the processing of the signals. Tests can be done on various frequency ranges, all using portions of the same test data. Unless special provisions are made, (i.e. using high sampling rates and large sampling times) purely digital test systems require additional tests if different frequency ranges are to be used. Another flexibility that this arrangement lends itself to is the fact that a multichannel FFT unit is not required to process the information. Instead, the analog data may be filtered and digitized with conventional equipment.

Privately developed or commercially available software can then be employed to reduce the data to yield the desired modal parameters. This approach allows a company or consulting firm to be able to do complete modal analysis with equipment (FM recorder, filters, digitizers and computing facility) that is usually already available. The complete modal analysis units on the other hand, tie up a lot of capital in a system that in many cases has limited flexibility and a short half-life before becoming obsolete.

1.3 Research Outline

The intent of this study was to investigate the flexibility of implementing a practical approach to modal analysis. This was to include both the writing of the data acquisition and modal analysis software as well as a description of what type of equipment is required to successfully carry out this procedure.

Chapter two of this report contains the formulation of transfer functions in the Laplace domain from the equations of motion for a structure. It also shows how results obtained from a Fourier transform of a time record relate to the Laplace domain representation of the body. This chapter concludes with a discussion on the limitations and assumptions of the discrete Fourier transform.

Chapter three deals with aspects of curve fitting the experimental data to the analytical representation of the transfer functions that were developed in the previous chapter. It shows how an approximate linear method can be used to generate good initial estimates for the modal parameters in question and how a simultaneous, multi-degree of freedom curve fit can be used to accurately complete the process. This is followed by a modal vector identification scheme that can deal with either normal or complex mode shapes.

The following section, Chapter four, addresses some of the practical considerations that one must be concerned with when using transfer function analysis. The first deals with

the types of excitation procedures commonly used and why transient testing was chosen in this study. This is followed by a discussion into the kind of equipment that is required to first of all record the field data, and later play back the signals to be digitized and analyzed. The final part of this chapter looks into the coherence function and its use in determining some properties about the quality of the generated signals.

Chapter five discusses the set-up and results of two experimental tests. The first test was done on a free-free beam to allow easy comparison between theoretically predicted and experimentally derived results. The second set of tests were done on an air compressor base as an example of a practical engineering application of the procedure.

The final chapter lists the conclusions to the study and points out possible areas of future research that stem from this project.

2. THEORETICAL CONSIDERATIONS

To understand the transfer function method of testing, this chapter begins with the development of the transfer functions from the equations of motion. It is then shown how certain properties of the set of transfer functions for the structure, allow greatly simplified testing techniques when employing this method.

2.1 Transfer Functions in the Laplace Domain

Consider a continuous structure whose dynamic behavior is to be determined. It will be modelled by a series of discrete masses interconnected with linear springs and viscous dampers. The motion of this configuration may then be described by a set of second order linear differential equations with constant coefficients. In the time domain, these equations would have the form:

$$[M]\{\ddot{x}(t)\} + [C]\{\dot{x}(t)\} + [K]\{x(t)\} = \{f(t)\} \quad (2.1)$$

where:

- $\{f(t)\}$ - applied forcing vector (nx1)
- $\{x(t)\}$ - resulting displacement vector (nx1)
- $\{\dot{x}(t)\}$ & $\{\ddot{x}(t)\}$ - first and second derivatives of $\{x(t)\}$ with respect to time (nx1)
- $[M], [C]$ & $[K]$ - mass, damping and stiffness matrices (nxn)

Although it is not necessary to do so, we will only consider the case where $[M], [C]$ and $[K]$ are symmetric

matrices with real valued elements (see Potter, [13]).

Taking the Laplace transform of equation (2.1) and considering the case where the initial velocities and displacements are zero, at $t=0$, it will follow that:

$$[M]\{x(s)\}s^2 + [C]\{x(s)\}s + [K]\{x(s)\} = \{f(s)\} \quad (2.2)$$

Defining the system matrix as,

$$[B(s)] = [M]s^2 + [C]s + [K] \quad (2.3)$$

equation (2.2) can be simplified to:

$$[B(s)]\{x(s)\} = \{f(s)\} \quad (2.4)$$

The transfer matrix of the system, $[H(s)]$, is defined as:

$$[H(s)] = [B(s)]^{-1} \quad (2.5)$$

Considering equation (2.3) and noting that,

$$[H(s)] = \frac{\text{adj}[B(s)]}{\det[B(s)]}$$

it is apparent that each element of $[H(s)]$ is a rational function of the Laplace variable, 's'. Therefore each term in the transfer matrix can be expressed in partial fraction form. The zeroes of the $\det[B(s)]$ (the poles of the transfer matrix) always occur in complex conjugate pairs except when the system is critically damped or over-damped (poles will be real valued in these situations).

 'Numbers in square brackets refer to references'

Assuming the poles are of unit multiplicity, $[H(s)]$ may be written as,

$$[H(s)] = \frac{[A_1]}{s-p_1} + \frac{[A_1^*]}{s-p_1^*} + \dots + \frac{[A_n]}{s-p_n} + \frac{[A_n^*]}{s-p_n^*}$$

or more simply as,

$$[H(s)] = \sum_{k=1}^n \left[\frac{[A_k]}{s-p_k} + \frac{[A_k^*]}{s-p_k^*} \right] \quad (2.6)$$

where: $[A_k]$ - complex residue matrix, $(n \times n)$

p_k - k^{th} pole of the system

n - total number of modes

'*' - denotes complex conjugate

2.2 Residue Matrix Properties

To determine some useful properties of the residue matrix $[A_k]$, equation (2.6) is pre-multiplied by the system matrix $[B(s)]$ and the scalar $(s-p_k)$.

$$(s-p_k)[B(s)][H(s)] = (s-p_k)[B(s)] \left[\dots + \frac{[A_k]}{s-p_k} + \frac{[A_k^*]}{s-p_k^*} + \dots \right]$$

From equation (2.5) we see that $[B(s)][H(s)] = [I]$ (the identity matrix), therefore the left hand side of the above equation reduces to $(s-p_k)[I]$. If we let $s=p_k$, the left hand side will be identically zero and the right hand side will be reduced to $[B(p_k)][A_k]$, therefore:

$$[B(p_k)][A_k] = 0 \quad (2.7)$$

In a similar manner, post-multiplying equation (2.6) by $[B(s)](s-p_k)$ and allowing $s=p_k$, it will be seen that

$$[A_k][B(p_k)] = 0 \quad (2.8)$$

Now consider equation (2.4) with the forcing function, $\{f(s)\}$, set equal to zero.

$$[B(s)]\{x(s)\} = 0$$

These homogeneous equations correspond to the free, damped vibration of the system. Non-trivial solutions will only exist if the $\det[B(s)] = 0$. For a value of 's' that satisfies $\det[B(s)] = 0$, say $s=p_k$, there will also exist a unique solution vector, $\{u_k\}$ such that:

$$B(p_k)\{u_k\} = 0 \quad (2.9)$$

$\{u_k\}$ is known as the modal vector or mode shape for the pole $s=p_k$.

If we now consider equations (2.7) & (2.8) in the light of equation (2.9), it can be seen that both the columns and the rows of the residue matrix $[A_k]$, must be linear combinations of the modal vector $\{u_k\}$. $[A_k]$ can then be replaced by,

$$[A_k] = \alpha_k \begin{bmatrix} u_1 \\ u_2 \\ u_3 \\ \vdots \\ \vdots \\ \vdots \end{bmatrix}_k [u_1 u_2 u_3 \dots]_k = \alpha_k \{u_k\} \{u_k\}^t \quad (2.10)$$

where ' α_k ' is a complex constant. In general the elements of the modal vector $\{u_k\}$ are complex. If however, the system is proportionally damped², the modal vectors will be purely imaginary. Substituting equation (2.10) into equation (2.6) yields,

$$[H(s)] = \sum_{k=1}^n \left[\frac{\alpha_k \{u_k\} \{u_k\}^t}{s-p_k} + \frac{\alpha_k^* \{u_k^*\} \{u_k^*\}^t}{s-p_k^*} \right] \quad (2.11)$$

Due to the properties of the residue matrix (equation (2.10)), it is only necessary to make measurements that will complete one row or column of the matrix to completely define the system. This can be accomplished by exciting the structure at one point and recording the response at all other points of interest (simultaneously or one at a time). Alternatively the response can be measured at one fixed point and then allow the forcing stimulus to be positioned at various points on the structure.

2.3 Frequency Response Function

Between any two points on the test structure, the transfer function can be found by forming the following operation,

$$H(s)_{ij} = \frac{X(s)_j}{F(s)_i}$$

where $X(s)_j$ is the Laplace transform of the response at a point 'j' due to the forcing function and its corresponding

²For a more general discussion, see Caughey [5].

Laplace transform, $F(s)$, at point 'j'.

For the purpose of this study, the complex variable 's', can be written as,

$$s = \sigma + j\omega$$

where ' σ ' is the damping coefficient and ' ω ' is the damped angular frequency. A complex pole of a system is written as

$$p_k = \sigma_k + j\omega_k.$$

The damping coefficient of a pole, σ_k , is negative for a stable system, and the natural frequency, ω_k , is actually the damped natural frequency for the particular mode. The undamped natural frequency (resonant frequency) is found from

$$\omega_{k n} = (\omega_k^2 + \sigma_k^2)^{0.5}$$

and the damping ratio is determined from

$$\zeta = \frac{-\sigma_k}{\omega_{k n}}$$

Both the real and imaginary components of the transfer function, $H(s)$, map out continuous surfaces over the Laplace plane (except at pole locations). To be able to fully describe the surfaces and represent them in the form of equation (2.11) it is not necessary to make measurements over the entire s-plane, because the surface is described by an analytic function.

In practice, the transfer functions are measured along the imaginary axis. What is in fact done is to evaluate a Fourier transform rather than a complete Laplace transformation. This is equivalent to letting $s=j\omega$ (i.e. $\sigma=0$) and computing the transfer function along this line. This representation of the transfer function is known as the 'frequency response function'. From these measured values, the entire s-plane representation may be formed if desired.

2.4 Discrete Fourier Transform

The Fourier transform is defined as;

$$G(f) = \int_{-\infty}^{\infty} g(t) \exp(-j2\pi ft) dt.$$

Practical limitations necessitate that the signal record be of finite duration, say from $t=0$ to $t=T$, such that;

$$G(f) = \int_0^T g(t) \exp(-j2\pi ft) dt.$$

The analog signals, that are to be analyzed, are normally digitized to allow efficient handling and processing of the data. This discretization, coupled with the time limited sample record, reduces the integral transform to a discrete Fourier transform of the form;

$$G(f_k) = 1/N \sum_{n=0}^{N-1} g(t_n) \exp(-j2\pi f_k t_n) \quad (2.12)$$

where 'N' is the number of samples of the time domain signal.

The 'windowing' in the time domain has the effect of limiting the maximum obtainable frequency resolution ($\Delta f = 1/T$). Any increase in frequency resolution for a given test must be accompanied with longer sampling times. The finite number of time sample points recorded (typically $N=1024$), limits the maximum obtainable frequency, f_m , that may be determined. The sampling period Δt , is given by

$$\Delta t = \frac{T}{N}$$

and f_m is found from

$$f_m = \frac{1}{2\Delta t} = \frac{N}{2T}$$

To obtain information in higher frequency ranges, shorter sampling periods must be employed. If N is to stay fixed however, this dictates lower (and often unacceptable) frequency resolutions. To alleviate this problem, 'zoom' transformations are used, which allow the operator to choose the upper and lower frequencies over which the Fourier transformation is to be performed. This then allows the available number of spectral lines to be used in a specific bandwidth of interest rather than from DC to some maximum frequency (see [12]).

2.5 Windowing

The digitizing of the time domain signals are subject to Shannon's sampling theorem which states that in order to avoid aliasing or 'folding back' in the frequency domain, the sampling rate must be greater than twice the highest frequency content of the waveform to be analyzed. By passing the signals through low-pass filters however, does not ensure that the frequency content above some designated frequency has been attenuated to zero. It would be necessary to sample at an infinite rate to avoid any aliasing for a general waveform. Sampling at a finite rate then, will involve folding back to some degree (except for a band limited function). Its effect however, can be safely ignored if the frequency content of the signal that is folded back is small compared to that in the frequency range of interest.

In typical waveform analysis, the analog signals are first of all passed through sharp roll-off, low-pass filters (the cut-off is set at the highest frequency of interest, f_m). These waveforms are then digitized at a rate of f_s , where $f_s > 2f_m$. Any frequency content of the signal greater than $f_s - f_m$ will be folded back to the frequency range in question. However if $f_s = 2.56f_m$ and the low pass filter has a roll-off rate of 96dB/octave, then the signal folded back onto the frequency f_m , would be attenuated by 62dB. This degree of suppression is normally more than adequate to take care of any potential aliasing problems.

Once the signals have been properly filtered and digitized, a discrete Fourier transform is performed on them. Examining equation (2.12) it is seen that the frequency domain, in addition to the time domain signal, is considered in a discrete rather than in a continuous sense. This is necessary because for digital computation, only discrete values of the frequency response function can be formed. It is shown in [3], that this 'uniform sampling' in the frequency domain implies that the time domain signal be periodic. This means that any time domain signal that is to be analyzed, must be representative of one period (or an integer multiple of it). If this is not true, significant distortion of the frequency spectrum may result. To reduce this effect, time domain windows are used, which force the signal to be periodic within the sample time. This is done by simply multiplying the measured, digitized signal by a function that tapers off to zero at either end of the window. A commonly used window in the study of continuous signals is the Hanning window, which has the functional form

$$w(t) = 0.5[1 - \cos(2\pi t/T)] \quad 0 \leq t \leq T.$$

Although this, or any other applied window, does not totally eliminate the distortion (the windowing process itself adds some predictable amount of distortion to the signal) caused by a finite time sample, the windowing reduces the distortion to a level from which meaningful results can be derived.

During the course of this study, impulse testing was employed as an exciting force in the determination of the transfer functions for a structure. This type of excitation resulted in transient waveforms for both the forcing and response signals. Typical experimental signals, that have been low-pass filtered, are shown in figures 2.1 and 2.2. When computing the Fourier spectrum, these transient waveforms require different windowing functions than those used with continuous signals. In fact, the input force signal does not even require a window because it is self-windowing (that is, it occurs completely within the allotted time block). The response signal on the other hand, which is composed of decaying sinusoids, may not have died out completely in the time record and must therefore be windowed. It is apparent that applying a Hanning window to this type of signal would not be appropriate, because in the process of forcing the signal to zero at both ends of the record, it has "lost" the majority of its information that was situated at the beginning of the time record. For this type of signal, an exponential window is used. A commonly used form of this window weights the data by a factor of one at the start of the window to a factor of 0.05 at the end of the time block. This can be expressed as,

$$w(t) = \exp(-\beta t)$$

where $\beta = \log(0.05)/T$. It should be noted that unlike the Hanning window, the exponential window does not force the

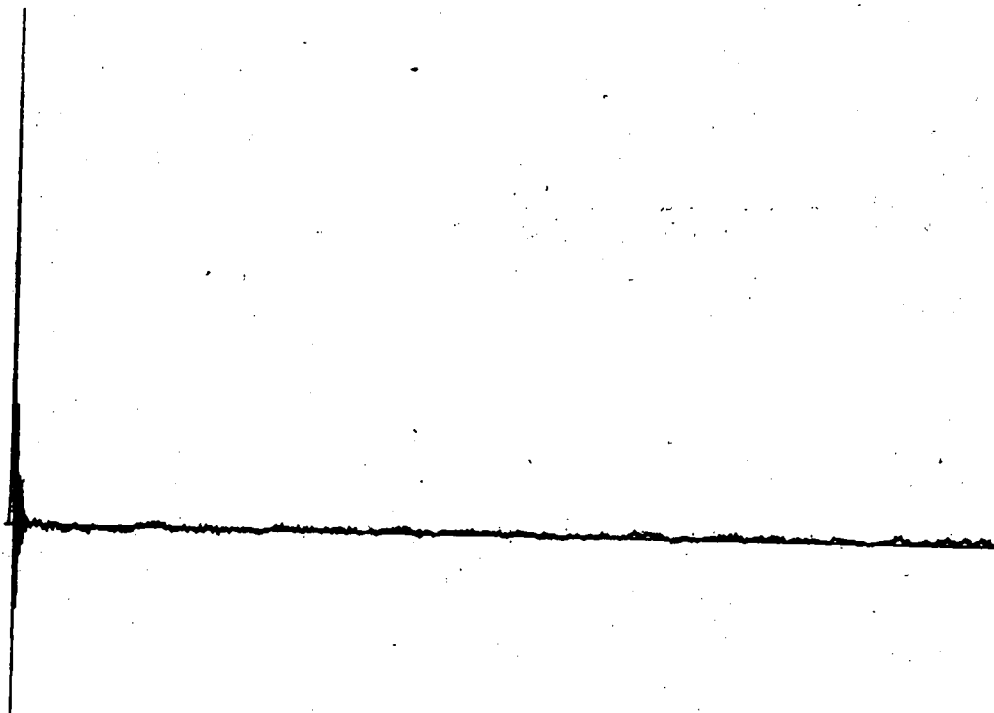


Figure 2.1 Forcing Signal

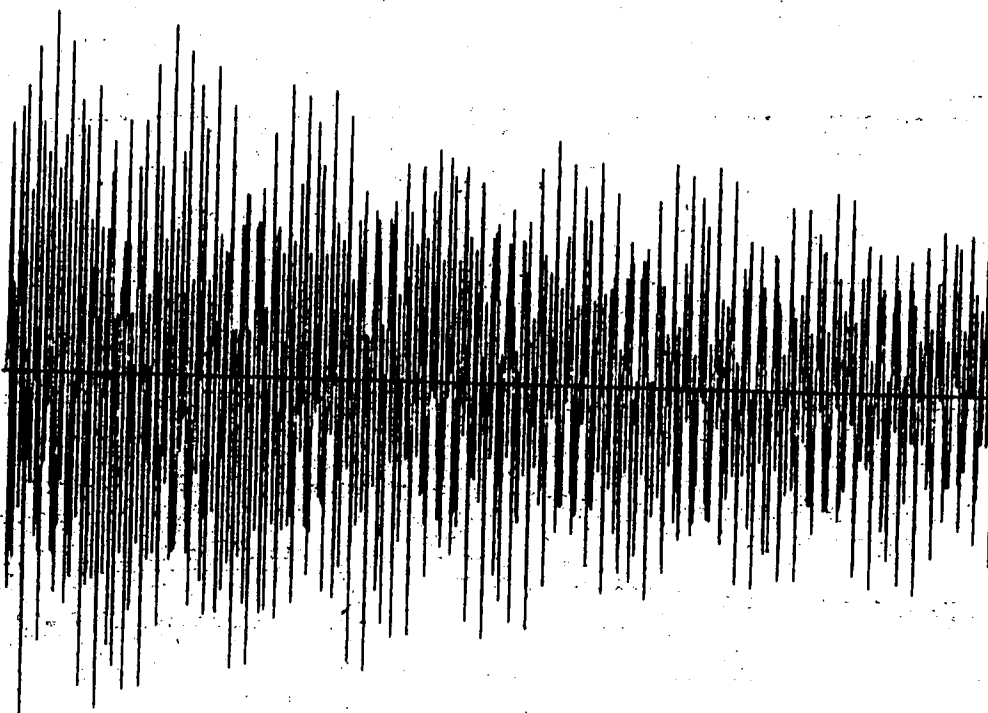


Figure 2.2 Response Signal

signal to be zero at both ends of the time record. The left-hand edge of the response signal is already zero due to the fact that the structure has not yet been excited, and so there is no need for weighting at this point. As the response signal continues in time, it decays exponentially and the effect of the window is to increase the apparent damping in the system, by bringing the right-hand edge of the signal as close to zero as desired. When the modal parameters are determined from the exponentially windowed response functions, the measured damping values (σ) will be the sum of the actual damping present in a particular mode and the amount of damping present in the window itself (β). To obtain the true damping for a mode then, it is only necessary to subtract the damping induced by the window from the total measured damping value. It should be noted that the apparent increase in damping induced by the exponential window, can cause tightly spaced, heavily damped modes to become very difficult to analyze and therefore may require additional tests with increased frequency resolution.

The exponential window has an additional feature which makes it even more useful as a windowing function of the response signals. This is due to the fact, that as the response signal becomes smaller at the end of the time record, the signal to noise ratio is significantly reduced (especially in heavily damped systems). This would tend to add unwanted noise into the signal. However, when the exponential window is applied, it most heavily weights the

signal at the beginning of the time block where the signal to noise ratio is highest, while the potentially noisy portion of the signal is largely suppressed.

As stated earlier, no windowing is necessary for the impulse forcing function to meet the 'periodic time domain' criteria of the discrete Fourier transform. Windowing is used on this type of signal however, to reduce the inherent noise in the signal that is due to the short duration of the impulse compared to the total sample length. A simple type of window that can be used is a rectangular function. With this window, the actual impulse portion of the signal, is given a weighting of unity and the data beyond that point is set to zero so that any stray noise in that section of the signal is removed.

3. IDENTIFICATION OF MODAL PARAMETERS

Once one row or column of the transfer function matrix has been measured, it is then necessary to determine the modal parameters (natural frequency, damping coefficient and mode shape) for each mode in the frequency range of interest. Assuming a linear model is valid for the test structure (as in equation (2.1)), the corresponding transfer functions may be represented by a simple sum of the response curves for each of the natural frequencies of the system.

Figure 3.1 shows an example of a transfer function (solid line) and its contributing single degree of freedom components. Notice that the net transfer function lies below some of its contributing components. At first this would appear to be an inaccurate summation. It must be remembered however, that the transfer function is complex valued and that the overall transfer function is the sum of the real and imaginary parts of the single degree of freedom systems (only the magnitude is shown in figure 3.1).

The density of the modes will dictate what type of analysis is necessary for extraction of these parameters. When the natural frequencies of the system are well spread apart and the damping is light, single mode methods are used which make use of the data in the immediate area of the resonance peak. On the other hand, a multiple-mode technique is required to separate and identify a system with tightly spaced peaks and large damping factors. Here it is necessary that all of the modal parameters be identified

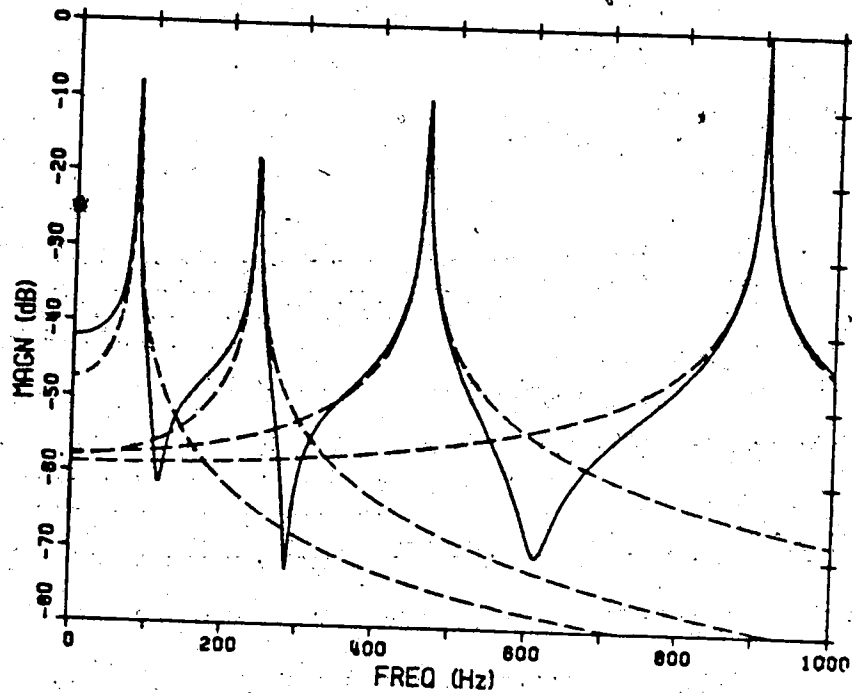


Figure 3.1 MDOF Transfer Function

simultaneously. The methods employed are often iterative in nature and the initial values for the parameters to be used in the computations are typically obtained from single mode approximations.

In modal analysis, the process of identification of a system is often termed 'curve fitting'. This is because experimental data is frequently fit (in a least-squares sense) to an analytical transfer function. A common function used to fit the data is shown below.

$$H(j\omega) = \sum_{k=1}^n \left[\frac{a_k}{j\omega - p_k} + \frac{a_k^*}{j\omega - p_k^*} \right] \quad (3.1)$$

This equation is obtained by substituting $s=j\omega$ into equation (2.6) (as the transformed experimental data is in the frequency domain) and by considering one element in the residue matrix $[A_k]$ (and the corresponding element in $[A_k^*]$). The non-linear nature of this function often makes it difficult to successfully carry out the identification schemes.

3.1 Levy Curve Fit

Generally, single mode methods are the simplest to implement due to approximations that can be made in estimating the parameters of equation (3.1). These techniques however are slow and often do not make use of all of the available data around the mode of interest to obtain a best possible estimate of the parameters. In addition to this, it was desired to employ a method that would work equally well in situations that would warrant either a single or multiple mode analysis.

To satisfy the above criteria, a complex curve fitting scheme devised by E.C. Levy was chosen to be used. (A short discussion outlining the major steps in the development of this technique will be presented, however an interested reader is encouraged to consult the original paper outlining the method [10].)

Levy's method rewrites the transfer function of equation (3.1) as a ratio of two frequency dependent complex polynomials. This takes the form,

$$G(j\omega) = \frac{A_0 + A_1(j\omega) + A_2(j\omega)^2 + \dots + A_n(j\omega)^n}{1 + B_1(j\omega) + B_2(j\omega)^2 + \dots + B_m(j\omega)^m}; \quad (3.2)$$

or more simply as,

$$G(j\omega) = \frac{N(\omega)}{D(\omega)}. \quad (3.3)$$

Let the actual experimental data at frequency ' ω_k ', be given as $H(j\omega_k)$. The error at this point is defined as:

$$e(\omega_k) = H(j\omega_k) - G(j\omega_k) = H(j\omega_k) - \frac{N(\omega_k)}{D(\omega_k)} \quad (3.4)$$

Utilizing conventional least-squares analysis on the error, $e(\omega_k)$, this would yield a system of simultaneous, nonlinear equations to be solved. Iterative techniques are generally involved which require good starting values and some degree of operator experience. To avoid this problem, the error is multiplied through by the denominator of the analytical function. This results in:

$$e'(\omega_k) = e(\omega_k)D(\omega_k) = H(j\omega_k)D(\omega_k) - N(\omega_k), \quad (3.5)$$

which is now a weighted error function. When the method of least-squares is applied to the modulus squared of this function, it results in a set of linear algebraic equations that can be easily solved for the coefficients $A_0 \dots A_n$, $B_1 \dots B_m$ (of equation (3.2)). While this type of approach at first glance looks very promising, it produces unsatisfactory answers when large frequency ranges are encountered or when the denominator term, $D(\omega)$, of the

analytical function has a wide range of values (like that which occurs near a pole). This is due to the weighting of the error function by the denominator term. It has been shown by Sanathanan and Koerner[20] that these effects can be virtually eliminated by a simple iteration to eliminate the weighting. The error function of equation (3.5) is modified to the following form:

$$e''(\omega_k) = \frac{e'(\omega_k)}{D(\omega_k)_{i-1}} = \frac{e(\omega_k)D(\omega_k)_i}{D(\omega_k)_{i-1}} \quad (3.6)$$

where the subscript 'i' corresponds to the iteration number. Because $D(\omega_k)$ is not initially known, it is set equal to one for the first iteration (i.e. the first iteration is identically the weighted least-squares minimization). Ensuing iterations converge very rapidly. Five to ten iterations are normally required to have the parameters agreeing to within 0.1% from one iteration to the next.

This technique proved to be very successful due to its speed, ease of application and agreement with the experimental data that it was meant to fit. The extraction of modal parameters with tightly spaced, adjacent modes were also correctly identified using this simultaneous curve fit. However, it strayed from the true parameter values when it was applied to fit two or more peaks simultaneously that were separated by a large number of data points. This was not found to be a problem because when the peaks were widely separated, they could be safely treated as single degree of freedom systems with little interaction from other modes. A

simultaneous fit was therefore not necessary.

When applying Levy's method, it must be decided how many terms of the numerator and denominator will be used in any particular curve fit. (see equation (3.2)) At first, one might select a large number of 'A' and 'B' coefficients and let the ensuing calculations determine how many of the terms were necessary (i.e. the terms that were not used in the fit would equal zero (or nearly so)). This 'blind' approach can lead to problems, because when many excessive terms are used, ill-conditioned numerical problems are frequently encountered. This problem need not occur however, because it is very straight forward to calculate the exact number of terms that should be used in the fit. For a single degree of freedom, the transfer function takes the form:

$$H(j\omega) = \frac{a}{j\omega - p} + \frac{a^*}{j\omega - p^*} \quad (3.7)$$

where: $a = a_x + ja_y$

$p = \sigma_0 + j\omega_0$

Substituting the expressions for 'a' and 'p' and putting everything over a common denominator, equation (3.7) can be written as:

$$H(j\omega) = \frac{-2(a_x\sigma_0 + a_y\omega_0) + (2a_x)j\omega}{\sigma_0^2 + \omega_0^2 - (2\sigma_0)j\omega - \omega^2} \quad (3.8)$$

Dividing both numerator and denominator by ' $\sigma_0^2 + \omega_0^2$ ', equation (3.8) could be written in the form

$$H(j\omega) = \frac{A_0 + A_1(j\omega)}{1 + B_1(j\omega) + B_2(j\omega)^2}$$

where A_0 , A_1 , B_1 , and B_2 are real constants that would be determined from the Levy curve fit. For each additional mode that is to be fit, it can be shown that it is necessary to add two additional terms to both the numerator and denominator. So that for two simultaneous modes, for example, it is necessary to determine the constants A_0 to A_3 and B_1 to B_4 .

Once the Levy coefficients have been determined, it is necessary to find the poles of the system, (i.e. to convert from the form of equation (3.2) back to that of equation (3.1). This is done by calculating the complex zeroes of the analytical denominator function (e.g. the zeroes of $1 + B_1(j\omega) + B_2(j\omega)^2 + B_3(j\omega)^3 + B_4(j\omega)^4$ for the two degree of freedom case). These zeroes typically occur in complex conjugate pairs, but they can be purely imaginary if the damping is zero. It is then a simple matter of performing a partial fraction expansion (using the computed poles) to finish the transformation. (Appendix A lists a Fortran program that computes a Levy curve fit and then converts the derived parameters to the partial fraction form.)

3.2 A True MDOF Curve Fit

If the curve fitting process has not included all of the modes of the structure (always the case for a continuous system) the curve fit will be inaccurate to some degree.

This is because the 'tails' of the modes outside the frequency range of interest, will have been measured during the data acquisition process, (there is no way to filter them out) but no terms were included in the curve fit procedure to account for them. To choose what type of function would best suit the tails of the modes outside the desired range, it is necessary to examine the transfer function for one mode. Rewriting equation (3.9) again:

$$H(j\omega) = \frac{A_0 + A_1(j\omega)}{1 + B_1(j\omega) + B_2(j\omega)^2}$$

it is seen for small values of ' ω ', that the transfer function may be represented by a real constant (in this case ' A_0 '). For large ' ω ' values on the other hand, the transfer function is proportional to $1/\omega^2$ (again real valued; note that the constant ' A_1 ' is zero when proportional damping is present or nearly zero when light, non-proportional damping exists).

If it is desired for example, to fit the modes in a certain frequency range (ω_1 to ω_2) of a transfer function and there exists other modes outside this range, the following analytical function would best represent what is occurring inside the range of interest.

$$H(j\omega) = \frac{C}{\omega^2} + \sum_{k=k_1}^{k_2} \left[\frac{a_k}{j\omega - p_k} + \frac{a_k^*}{j\omega - p_k^*} \right] + D \quad (3.10)$$

where ' ω ' is restricted to $\omega_1 \leq \omega \leq \omega_2$, and the modes from ' k_1 ' to ' k_2 ' are also located in this range. The term ' C/ω^2 '

would take care of the effects of the tails of any modes below ω_c , and the constant term, 'D', would similarly compensate for those modes above ω_c .

With this analytical model to work with, a method must be devised to correctly identify the constants in the expression. Ideally all of the parameters of equation (3.10) should be identified simultaneously and preferably using a least-squares technique to smooth out the effects of any random error. Because of the nonlinear nature of this problem, good starting values (initial guesses) are necessary to increase the likelihood of convergence in the iteration scheme. As previously noted, Levy's method gave a good approximation to the modes within the range without including the effects of the modes outside the range (i.e. the term $C/\omega^2 + D$), and therefore would give good starting values for the terms a_k and p_k (remembering that the subscript 'k' indicates the k^{th} mode in the range of interest). To initialize 'C' and 'D', the difference is now formed between the experimental data and the Levy curve fit model. The real part of this complex difference is curve fit to the function $C/\omega^2 + D$. Although this fit may not give accurate estimates of 'C' and 'D', it at least gives reasonable starting values to the two parameters.

All of the parameters of equation (3.10) have now been assigned starting values for use in the simultaneous curve fit. The error function, ϵ , that is to be minimized using the least-squares technique, is normally defined in the

following way:

$$\epsilon = \sum_{m=s}^t ||H(j\omega_m) - H_{exp}(j\omega_m)||^2$$

where: $H(j\omega_m)$ - analytical transfer function
(e.g. equation (3.10))

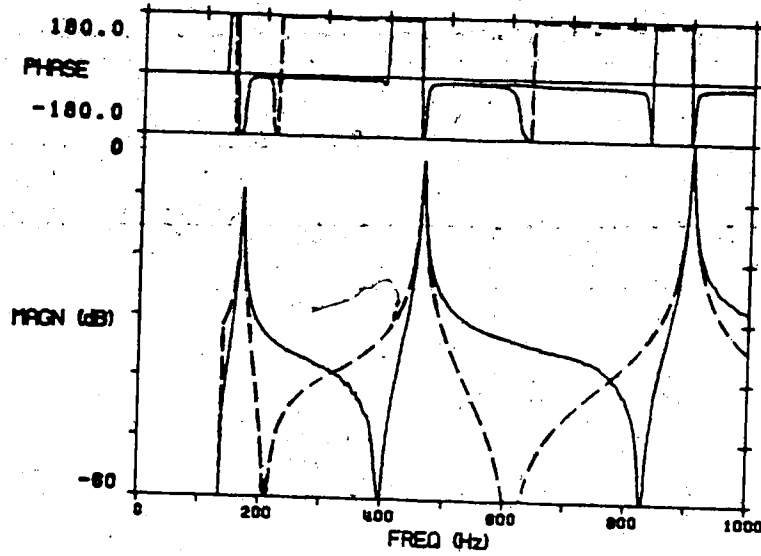
$H_{exp}(j\omega_m)$ - experimental transfer function

'|| ... ||' - indicates modulus

The minimization can now take one of several routes; it can proceed in a purely iterative fashion with all of the parameters optimized this way or, the minimization can go back and forth between solving for the parameters 'a_k', 'C' and 'D' in a linear fashion and for the parameters 'p_k' with an iterative approach. If some values of the parameters are known to be accurately determined, these can be held fixed while minimizing with respect to the other variables.

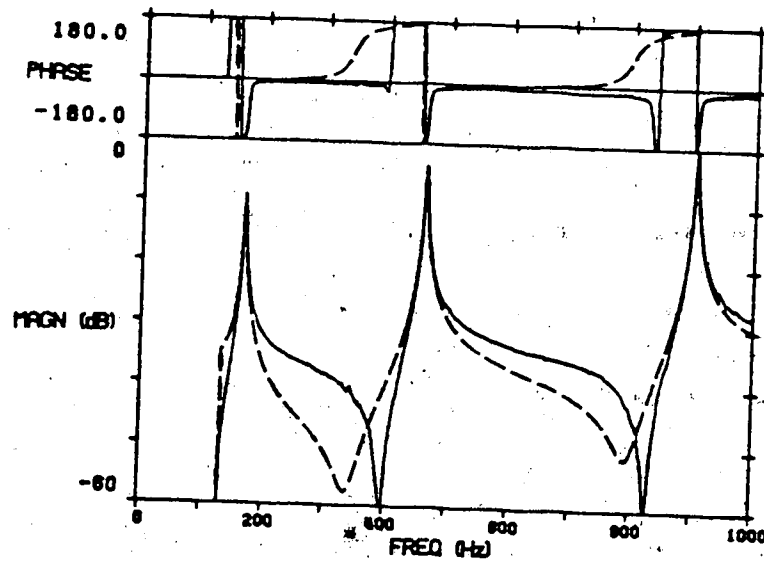
In this study, the first of these three methods was chosen due to the ease in programming, that is, performing the minimization of all of the parameters with an iterative approach. This method of computation was fairly costly in terms of computer time and it is suggested that the second and third methods could be employed to speed up the process.

The following three figures show the typical progress of a curve fit using the above outlined procedure. Figure 3.2 shows the results of the initial Levy approximation (the solid line indicates the experimental data). The transfer function curves are only shown in the frequency range of the



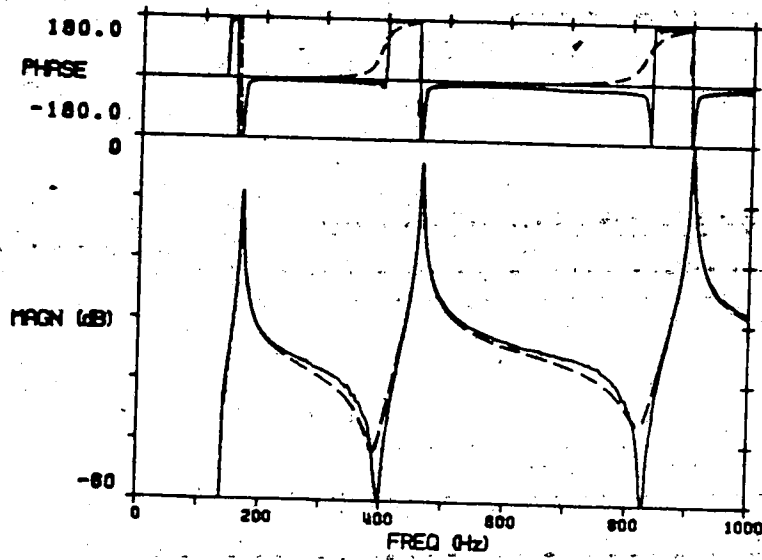
TEST PT. 1 FREE-FREE BEAM

Figure 3.2 Levy Curve Fit



TEST PT. 1 FREE-FREE BEAM

Figure 3.3 Levy Curve Fit and Additional Terms



TEST PT. 1 FREE-FREE BEAM

Figure 3.4 True Least-Squares Curve Fit

curve fit because it is only in this range that the curve fit is valid. Figure 3.3 is the same as figure 3.2 except that it now includes the preliminary estimates of the coefficients in the term ' $C/\omega^2 + D$ '. Notice the apparent 'vast improvement' in the fit, just due to the addition of this term. At this point, the fit is not expected to be perfect, even though all of the terms of the analytical function (equation (3.10)) have been assigned values. This is because these coefficients are estimates only, and were not calculated simultaneously.

The final stage of the curve fitting procedure is the simultaneous least-squares minimization of the error function, equation (3.11), with respect to the parameters ' a_k ', ' p_k ', ' C ' and ' D '. As can be seen in figure 3.4, the analytical curve fit falls very closely beside its experimental counterpart.

The largest differences between the two occur where the curves reach their minimum values. At these locations, the magnitude of the error is small (though it appears large with the log scaling) and therefore has little effect on the simultaneous curve fit. If an improved fit is desired, weighting would be necessary to emphasize the errors in these regions of the graph.

3.3 Mode Shape Determination

The final curve fit parameters of equation (3.10) describe an experimental transfer function. The values obtained however, offer little insight into the problem at hand unless they are compared to, and used with, other transfer functions obtained from different testing points. The relationship between the transfer function parameters will become clearer in the following discussion.

As noted in the previous chapter, the properties of the residue matrix $[A_k]$ made it necessary to only determine one row or column of the transfer matrix $[H(s)]$. Rewriting equation (2.4) as:

$$\{x(s)\} = [B(s)]^{-1}\{f(s)\}$$

and substituting equation (2.5), results in

$$\{x(s)\} = [H(s)]\{f(s)\}$$

To determine one row of the transfer matrix it would be necessary to measure the response at one point on the structure, due to forcing functions being applied, one at a time, to all of the other points of interest on the structure, i.e.

- H_{11} from response at point 1 due to force at point 1
- H_{12} from response at point 1 due to force at point 2
- etc.

In a similar manner, one column of the transfer matrix would

be determined by forcing the structure at one point and measuring the response at all other desired points on the structure (simultaneously or one at a time).

In determining one row of the transfer matrix, for example, one row of each of the residue matrices have necessarily been determined. Consider a two degree of freedom system.

$$H(s) = \begin{bmatrix} \frac{a_{11}^{(1)} + a_{11}^{(1*)}}{s-p_1} + \frac{a_{11}^{(2)} + a_{11}^{(2*)}}{s-p_2} & \frac{a_{12}^{(1)} + a_{12}^{(1*)}}{s-p_1} + \frac{a_{12}^{(2)} + a_{12}^{(2*)}}{s-p_2} \\ H_{21} & H_{22} \end{bmatrix}$$

where the 'a' and 'p' values are complex constants determined from the curvefit. This can be written as

$$H(s) = \frac{\begin{bmatrix} a_{11}^{(1)} & a_{12}^{(1)} \\ ? & ? \end{bmatrix}}{s-p_1} + \frac{\begin{bmatrix} a_{11}^{(1*)} & a_{12}^{(1*)} \\ ? & ? \end{bmatrix}}{s-p_1^*} + \frac{\begin{bmatrix} a_{11}^{(2)} & a_{12}^{(2)} \\ ? & ? \end{bmatrix}}{s-p_2} + \frac{\begin{bmatrix} a_{11}^{(2*)} & a_{12}^{(2*)} \\ ? & ? \end{bmatrix}}{s-p_2^*} \quad (3.11)$$

where the symbol '?' represents those values that were not determined from testing. Using equation (2.10), the first residue matrix can be represented by

$$[A_1] = \begin{bmatrix} \alpha_{1u_1u_1} & \alpha_{1u_1u_2} \\ \alpha_{1u_2u_1} & \alpha_{1u_2u_2} \end{bmatrix} \quad (3.12)$$

Matching common terms from equations (3.11) and (3.12), it is seen that

$$a_{11}^{(1)} = \alpha_1 u_1 u_1 \quad \text{and}$$

$$a_{12}^{(1)} = \alpha_1 u_1 u_2$$

The components of the modal vector u_1, u_2 are relative quantities and may be calculated any number of ways (α_1 is a complex constant and u_1, u_2 are the complex mode shape vectors). Dividing $a_{11}^{(1)}$ by itself, yields a real number of unity value. Dividing $a_{12}^{(1)}$ by $a_{11}^{(1)}$, produces a complex number that is a ratio of u_2/u_1 . The form of this ratio specifies the nature of relationship between u_2 and u_1 . If the ratio is real valued, a normal mode is present. The sign of this real number, positive or negative, indicates whether u_2 is in phase or out of phase with u_1 , respectively. If the ratio is zero, it indicates that the test point is a nodal point for the mode in question. If forming this ratio results in a complex number, it indicates that a complex mode is present. A complex mode indicates that when the structure is vibrating in that mode, that all points on the structure will not reach their minimum or maximum values simultaneously. It also indicates that nodal points on the structure will not be stationary. They will have to be thought of as instantaneous nodal points. The complication of the complex modes can usually be ignored when studying lightly damped structures as modal vectors will only stray slightly (a 5 or 10 degree phase shift) from being totally real valued.

If this normalization process is done individually for every mode, the relative amplitudes of the modes will not have been taken into account. Compared to the lowest frequency modes, higher order modes typically have much smaller dynamic deflections, due to larger internal damping of the more complicated mode shape. Calculating the relative deflections of the modes in a structure can be done by comparing the modal parameters between modes on a point by point basis. If the 'inertance form' (acceleration/force) of the transfer function was used in the modal parameter extraction, it must be remembered to divide the residue values by a factor of $(2\pi f)^2$ to convert these numbers to their equivalent 'dynamic compliance' representation, from which the amplitudes can be derived.

4. PRACTICAL CONSIDERATIONS

Implementation of the transfer function method of testing, involves the simultaneous recording and analyzing of the forcing and response signals between designated pairs of points on the structure. This chapter deals with the three aspects of testing that were considered before and during the actual test measurements. The first section deals with the selection of the type of loading that was used to force the structures. This is then followed by a discussion of how field data was recorded employing commonly available scientific equipment. The final section deals with coherence and its role in verifying the test measurements.

4.1 Choice of Loading

There are many types of loading that may be applied when making transfer function measurements. These methods fall into three major categories.

- 1) Sine wave excitation
- 2) Random loading
- 3) Transient testing

The use of sine wave testing has been used successfully for over 30 years. Among its early uses were applications in the aerospace industry for determining modal parameters of aircraft wings. Sinusoidal testing is typically applied in one of two methods. In the first, one frequency is excited at a time and the response is measured once steady-state conditions have been reached to determine the gain and phase

shift. The alternative method is a swept sine approach, where the structure is forced through a certain frequency range and the response to this input is simultaneously recorded. Sinusoidal testing offers the advantages of only requiring analog equipment and the ability of taking accurate measurements because the excitation energy can be confined to as small a frequency band as desired. Its disadvantages include; long testing times, problems with low frequency excitation, and the need to set-up, align and use shaker tables (costly and cumbersome).

Random loading is capable of broad frequency range excitation using random signals to drive shaker tables. If desired, this random signal may be band-pass filtered to allow controlled excitation as was the case with swept sine loading. Although random testing similarly suffers from the need to use shaker tables and the fact that windowing must be used because it is not periodic in the time record, it does offer the advantage that averaging can be used to reduce non-linear effects in the structure and noise in the signal.

Transient testing, and in particular impact loading, offer a simple method to determine the response of a structure. Loading is commonly accomplished with an instrumented hammer (a hammer having a load cell mounted inside the head) which makes it very portable and easy to employ for field applications. The impulsive nature of the

'some signal generators produce 'periodic-random' signals that alleviate this problem

forcing function produces a broadband excitation signal and is to some extent controllable by changing the characteristics of the hammer head. Problems with this type of loading include: low energy densities in the upper frequency ranges, problems with non-linear response of the structure and noisy measurements due to the low signal to noise ratio as the signal dies out. Despite these drawbacks, the impulse testing method was chosen because of its simplification of the testing process, both in the amount of equipment required and amount of time needed to set up and use it.

4.2 Selection of Transducers and Calibration

Before any field tests were done, it was necessary to consider several factors. The size and sensitivity of the hammer and response accelerometer were chosen in light of the nature of the problem to be studied. For example, a light hammer (200 gm.) and a medium sensitivity (10 mV/g) pick-up was chosen for the beam test, while a massive hammer (5.5 kg.) and a sensitive accelerometer (80 mV/g) was required for the compressor base test (low frequency).

In the tests that were conducted, it was only desired to determine the natural frequencies, modal damping ratios and relative mode shapes of the structure in question. It was therefore not necessary to calibrate the hammer and accelerometer. Generally however, this calibration would be done before tests were carried out to allow one the option

of performing a detailed quantitative study of the test results if desired (e.g. actual dynamic deflections or determining the mass, damping and stiffness matrices from the derived modal parameters).

4.3 Test Point Determination

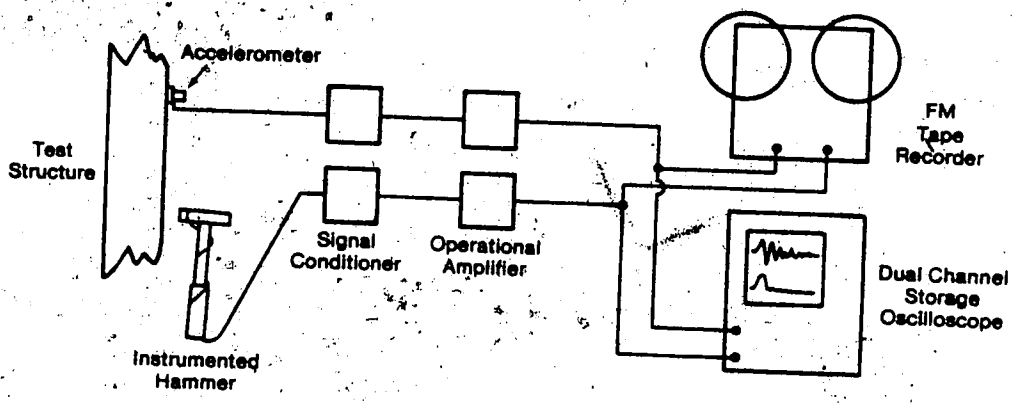
The complexity and size of the structure dictates the number of points on the structure to be tested. For the free-free beam, thirteen test points were chosen on one-half of the beam to get a good definition of the mode shapes. Here, use was made of the symmetric nature of the problem to reduce the number of test locations required. For the compressor base test, again only a minimum number of test points were necessary because of the rigid body nature of the vibration. Extra test points were included to test the validity of the mode shape assumptions. These measurement points were chosen so as not to include any suspected nodal points of the modes in the frequency range of interest. In this way, the derived transfer functions all contained the same number of modes and better global averages of the damping and natural frequency could be made. The test points were well marked to facilitate a consistent impact location and their position on the structure was recorded.

4.4 Equipment and Testing

Figure 4.1 shows a schematic diagram of the set-up for recording test data on tape.

The outputs of the instrumented hammer and response accelerometer were first fed into their own signal conditioners and then into an amplifier set to boost the signals to fill up as much of the usable voltage range of the tape recorder as possible (1 volt RMS). To further increase the signal to noise ratio, the signals could be passed through low-pass filters (not shown). In this way, only signals in the frequency range of interest would be recorded. This would increase the signal to noise ratio in a given frequency range, however it would not allow further analysis at a higher frequency range without taking more measurements. Most FM tape recorders have a signal to noise ratio of about 40 dB which limits the dynamic range of the measurements. As well, very high taping speeds must be used with these recorders if it is desired to capture high frequency signals (in the recorder used, a tape speed of 60 in/sec was necessary for a flat frequency response to 20,000 Hz). If low frequency information is not of interest (i.e. that below 20 or 30 Hz) direct recording can be used. It offers the advantages of higher signal to noise ratios and excellent frequency response at low tape speeds (50 to 19,000 Hz @ 3 3/4 in/sec).

To ensure that only good signals were recorded, a two channel storage oscilloscope was used to monitor the tests.



- Accelerometer - PCB Piezotronics Model 302A
- Hammer - PCB Piezotronics Model 208 A03
- Signal Cond. - PCB Piezotronics Model 480A
- FM Tape Recorder - Ampex Model FR 1300A
- Scope - Hewlett-Packard Model 141B
- Operational Amp - Custom

Figure 4.1 Equipment used to Record Data

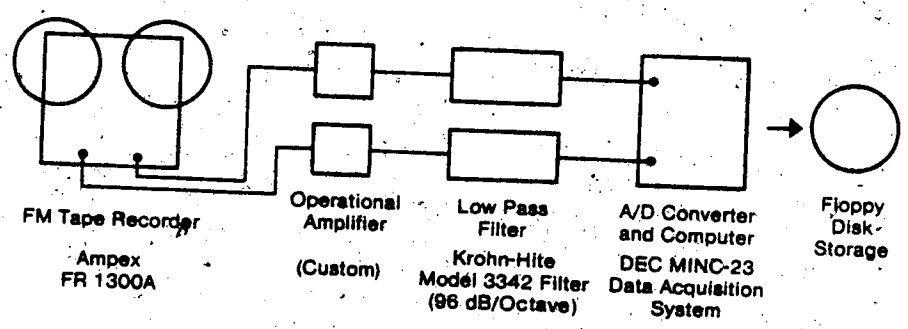


Figure 4.2 Equipment used to Digitize Signals

This is particularly important when tape recording impulse signals. When using a hand-held hammer to excite a structure, it is difficult to maintain a constant force from one run to the next; therefore some strikes will be too weak and have a poor signal to noise ratio, while others could be too large and saturate the tape. Another problem often encountered, was that of multiple impacts between the hammer and the test structure. This occurred when a mode with a large amplitude was excited and the structure rebounded against the impactor before it could be removed. This type of loading (quasi-periodic) often causes zeroes in the force spectrum (i.e. low signal to noise ratios at those locations) and therefore the runs were rejected.

In actual testing a minimum of averaging (4 averages per point) was done on each point to take further advantage of the time saving that is inherent with this impulse loading method. During both the free-free beam and compressor base tests, it was found to be important to allow some time between each impact to ensure that the structure had completely stopped vibrating from the previous excitation. If this was not done, the coherence between the runs would have been affected as the response measured from the ensuing impact would not have been solely due to that impact (see discussion on coherence later in this chapter).

4.5 Digitization of Signals

Once field measurements were complete, the recorded signals were digitized for processing. Figure 4.2 shows the arrangement of the equipment used in digitizing the data for this study. The output of the tape recorder was first amplified to fill the largest amount of the full scale range of the analog to digital (A/D) converter as possible (the digitizer used had only one voltage range; ± 5 volts maximum). The signals were then passed through anti-aliasing filters (sharp roll-off, low pass filters @ 96 dB/octave) and then into A/D converters. This data was labelled and put on floppy disks for further processing (curve fitting, etc.). With the particular digitizer used, the digitization was not truly simultaneous between channels. This type of situation could have distorted the original relationship between the signals, however owing to the sampling rates that were used, this problem was safely ignored (see Appendix B).

4.6 Coherence

The development of the transfer function relations in Chapter 2 assumed that the measured applied forces to the structure were its only inputs and that the response was due solely to this input. In practical testing however, the recording instruments have their limitations and test objects can not be totally isolated from external influences so that this condition is not completely met. Typical causes

for this include, electrical noise, limited dynamic range of the recording instruments, non-linearities in the transducers and the structure as well as vibration induced from the surroundings (e.g. rotating machinery, busy roads).

In order to measure the effects of these external influences, the coherence function, γ^2 , was used. This function can be calculated from the following expression

$$\gamma^2(f) = \frac{G_{xy}(f) G_{xy}^*(f)}{G_{xx}(f) G_{yy}(f)}$$

where $G_{xx}(f)$, $G_{yy}(f)$ and $G_{xy}(f)$ are the averaged input and output power spectrums and cross spectrums respectively (the star denotes complex conjugate). The coherence function which can only take on values between '0' and '1', can be thought of as a measure of the power in the response signal caused by the power in the recorded input. If the coherence equals one at some frequency, it implies that the output power at that frequency was entirely due to the measured forcing signal. When the coherence function takes on a value other than one, it shows that the system response at these frequencies was not totally due to the input.

Ideally then, the coherence function should equal one over the entire frequency range of interest. By graphically displaying this function along with the determined transfer function, serves as a valuable aid in determining certain properties about the recorded signals. In the tests that were done during this study, drops in coherence could invariably be attributed to the small dynamic range of the

FM tape recorder. Figure 4.3 shows a typical transfer function obtained from compressor base tests. In this diagram, it is seen that wherever the frequency content falls approximately 35dB below the peaks in the spectrum, that both the transfer and the coherence function are affected. In these regions the transfer function is no longer a smooth curve and is almost random in nature. This is due to the fact that an FM tape recording system has a dynamic range of about 35 to 40dB. When signals are recorded with a larger dynamic range than this, the smaller amplitude signals will not be recorded. This also causes the coherence to become very jagged, because in these frequency ranges the true signals were not recorded and what remains is a noise floor from the tape.

In the tests conducted, it was not necessary to have a large dynamic range so that the recording means was satisfactory. If a larger dynamic range is required several options can be considered. First, the tape recording aspect of the field data can be totally eliminated by directly digitizing the signals on location. Employing a twelve-bit A/D converter, a 72dB dynamic range can be realized. Secondly, if the flexibility of tape recording is desired and low frequency signals are not expected in the results, direct recording can be used. Typical direct (AC) recording systems have dynamic ranges in excess of 70dB and have large frequency bandwidths. When low frequency tape recording is necessary, a third alternative is the use of an FM tape

recording system that employs a switching unit to record one signal on two channels of the tape. One channel records that portion of the signal that lies in the zero to -35dB range while the second channel records anything below the -35dB level.

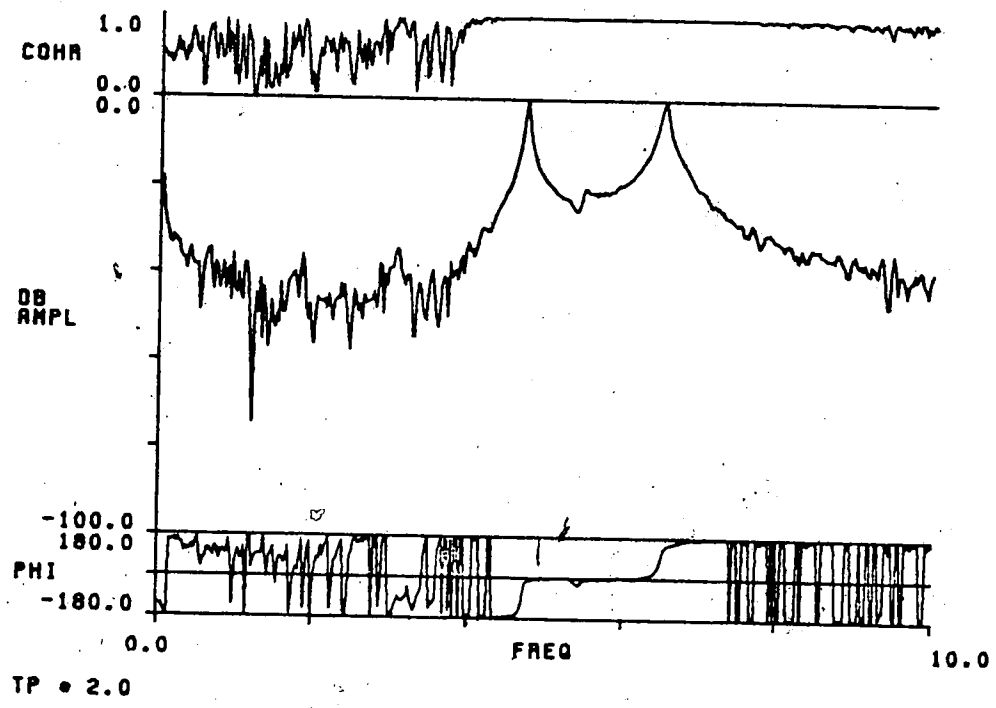


Figure 4.3. Coherence of Tape Recorded Signal

5. TEST RESULTS

In the two previous chapters, the procedure for determining the modal parameters as well as an outline for collecting experimental field data was presented. In this chapter the details of tests conducted on a free-free beam to verify the developed procedure are given. As well, results of an application of this technique to the dynamic analysis of an air compressor and its inertia base are included.

5.1 Free-Free Beam

A free-free beam was chosen for testing because of the potential ease of simulating the boundary conditions. A cantilever beam was considered, but in preliminary testing it was found that the measured response and corresponding frequency spectrum contained extraneous signals that could be attributed to the 'built in' support. This would not have caused any problems in the analysis of the derived transfer functions, but it was desired to do the first modal test on a structure that gave the cleanest signal possible.

A hot-rolled steel bar of dimensions 9.46 mm. x 37.4 mm. x 539.3 mm. was used as the test beam. Calculations showed that three natural frequencies for this bar (excluding rigid body modes) existed below 1000 Hz. Three widely spaced natural frequencies with low damping, was deemed a good starting test for the analysis system. The free end conditions for the bar were simulated in early

tests by placing the bar on a foam support. Two major problems were encountered using this technique. The first problem was that it was very difficult to impact the beam and pull the hammer away before the beam would bounce back and again make contact with the hammer. The discussion in the previous chapter pointed out why this type of signal was a problem. The second problem encountered using the foam base, was the very high damping induced by the support. In the analysis, this effect showed up as high modal damping parameters which were not expected in a steel structure. To overcome both of these problems, the bar was suspended by elastic bands at both ends. These low frequency supports induced rigid body modes that had natural frequencies in the order of 2 to 3 Hz; well below the frequency range of interest.

Because the study was to be restricted to those modes below 1000 Hz, it was not desirable to put any energy into the higher frequency ranges that were not to be analyzed, since this would lower the signal to noise ratio in the testing range. To meet this requirement, a hard rubber impact tip was used with the hammer. The resulting input signals had a spectrum that was flat ($\pm 3\text{dB}$) to approximately 1300 Hz and decayed gradually beyond this range.

From Chapter Two, it was seen that it is necessary to define one row or column of the transfer matrix to be able to completely describe the dynamic behavior of a structure. This is equivalent to taking measurements with a fixed

response pick-up and moving the force input to the desired locations on the structure (row determination) or fixing the forcing location and changing the position of the output transducer (column determination). In this test, it was chosen to rigidly mount the accelerometer at one end of the beam and impact the structure in different locations along its length because of the ease in moving the hammer from position to position. Only one half of the beam was tested due to the symmetry of the bar and its support conditions.

By mounting the accelerometer at the end of the beam, it was assured that the response of the beam would contain components of the lowest three modes in question, as all three have large modal deflections in this region. If the accelerometer had been placed at a node of one of the modes that it was desired to analyze, the response of that mode would not have been picked up, irrespective of where the beam was excited.

To choose the forcing locations along the beam, a single channel FFT analyzer was used to monitor the response to different impact locations. At locations where all three modes were present, a piece of tape was used to mark the location. If a nodal point for one of the modes was located, positions were tried on either side of the original spot until a suitable area was found. In the end, a total of thirteen impact locations were located on the one half of the beam at approximately 20 millimeter intervals. (It is important to note here that, this trial and error type of

approach for finding suitable test locations is somewhat slow and cumbersome and resulted from the lack of foresight in the original program development that analyzed the experimentally determined transfer functions. Generally however, testing points could be chosen arbitrarily and the analysis programs employed would account for the fact that a particular mode of vibration might have a nodal point at the location in question.)

As was mentioned in the previous chapter, an FM tape recorder was used to record the input and response signals. In these particular tests however, a direct recording unit would have been sufficient as there was no low frequency information (below 20 Hz) that was of interest.

Table 5.1 lists the averaged damping ratios and resonant frequencies determined from the tests and compares these resonant frequencies to those predicted theoretically for a free-free beam. The low damping ratios correspond with those typically observed in steel structures. For all three modes, the predicted frequencies are larger than the experimentally determined numbers. Comparing the ratios of f_n/f , however, very good agreement is seen. This indicates that the two cases differ by a scale factor. This scale factor may simply be due to the difference in the material constants (Young's modulus and mass density) and geometry of the bar compared with those assumed in the theoretical calculations.

	MODE 1	MODE 2	MODE 3
EXPERIMENTAL			
Damping Ratio (%)	0.144	0.100	0.094
Resonant Frequency (Hz)	167.29	462.22	905.61
f_n/f_1	1.000	2.763	5.413
THEORETICAL			
Resonant Frequency (Hz)	170.52	470.09	921.58
f_n/f_1	1.000	2.757	5.404

Table 5.1 Experimental vs. Theoretical Resonant Frequencies for the Free-Free Beam

TEST POINT	MODE 1		MODE 2		MODE 3	
	MAGN.	PHASE	MAGN.	PHASE	MAGN.	PHASE
1	1.000	0.0	1.000	0.0	1.000	0.0
2	0.835	-4.1	0.690	-4.0	0.511	-4.8
3	0.619	-0.5	0.344	-2.4	0.074	25.6
4	0.417	2.0	0.054	38.8	0.291	170.5
5	0.218	6.0	0.252	173.1	0.612	178.5
6	0.074	26.2	0.413	178.0	0.775	-176.2
7	0.113	165.6	0.564	178.7	0.743	-175.6
8	0.238	174.0	0.633	179.4	0.557	-174.4
9	0.348	175.3	0.681	-179.5	0.292	-175.8
10	0.429	176.3	0.577	-179.5	0.093	-2.4
11	0.487	176.8	0.443	-178.4	0.456	3.7
12	0.546	-179.9	0.292	-172.2	0.760	9.2
13	0.566	177.4	0.081	-174.0	0.832	4.6

Table 5.2 Normalized Modal Vectors for the Free-Free Beam

The experimentally derived, normalized mode shapes are given in table 5.2. Examining the phase angles of the modes, it is seen that parameters very nearly describe normal modes; that is, the modal vectors are either in phase with each other (phase angle near zero), or directly out of phase with one another (absolute value of the phase angle close to 180°). Figure 5.2, compares the experimentally determined mode shape (disregarding the imaginary component of the normalized modal vectors) to that given from the solution of the analytical equation. It is seen that the experimentally determined mode shapes agree very closely with their predicted behavior. (It should be noted that all three mode shapes have been normalized relative to the corresponding modal parameters of the first point on the beam. In doing so, the relative amplitudes of the modes have not been considered).

5.2 Compressor and Base

The second set of tests were performed on an 'Atlas Copco' air compressor and inertia base system that was designed to run at 720 rpm (12 Hz). The air compressor was driven by an electric motor with a pulley drive. The motor-pulley system and air compressor were mounted on a steel base filled with iron shot. The total mass of this system was approximately 3100 kg. with 580 kg. due to the compressor alone. The configuration was isolated from the floor by 4 steel springs, each with a stiffness of

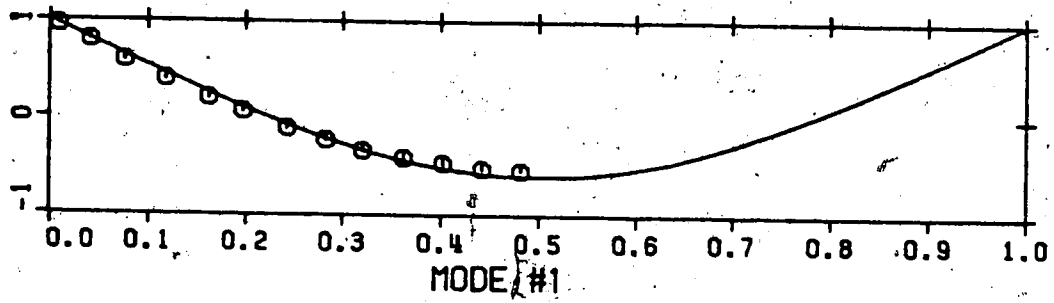


Figure 5.1 Mode Shape of the 167 Hz Mode

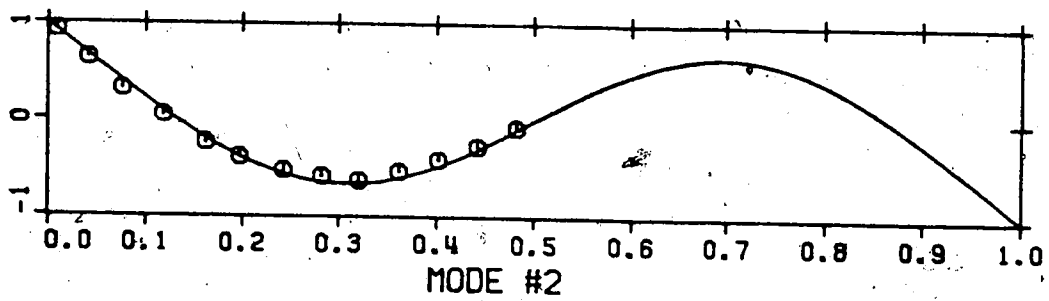


Figure 5.2 Mode Shape of the 462 Hz Mode

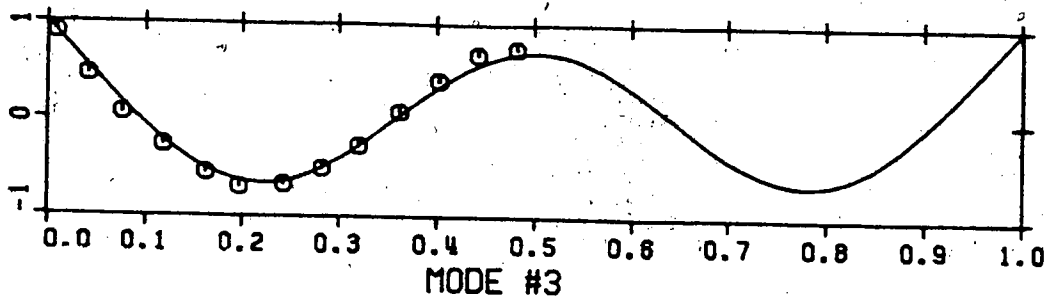


Figure 5.3 Mode Shape of the 906 Hz Mode

approximately 670 kN/m.

The simplest model of this setup would be that of a rigid body, free to move in all directions. This model would imply that six rigid body modes should be present in the structure. If the mass and stiffnesses were symmetric in all three planes, these modes would be uncoupled as shown in figure 5.4.

Any non-symmetries in the structure would tend to couple the modes in such a way that a mode would no longer be purely translational or rotational, but rather some combination of the three translational and three rotational motions. Because of the potential coupling, it is possible that all six modes could have been excited from one loading direction. However, small amplitudes resulting from any weakly coupled modes could have made the identification of reliable modal parameters difficult to obtain. It is also quite possible that some modes would not have been excited at all in the particular direction of loading considered and therefore not detected in the results. With this in mind, it was chosen to excite the body from three different test locations; one in each of the three principal planes. In this way the chances were good that all of the modes would be excited from at least one of the forcing locations (unless the three loading points happened to lie on a node of one the modes in question).

The testing points on the compressor system are shown in figure 5.5. The thick arrows (labelled 'A', 'B' and 'C')

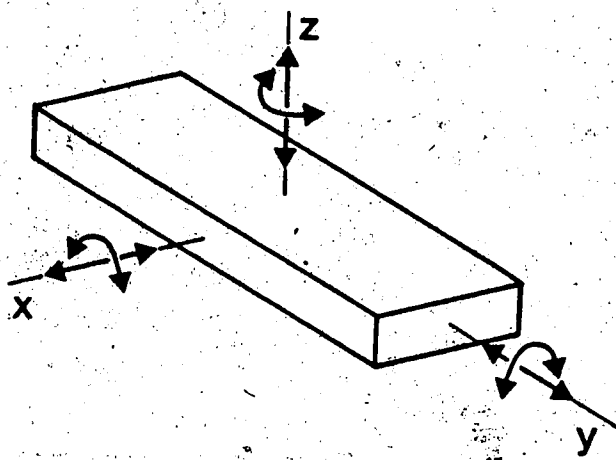


Figure 5.4 Six Rigid Body Modes

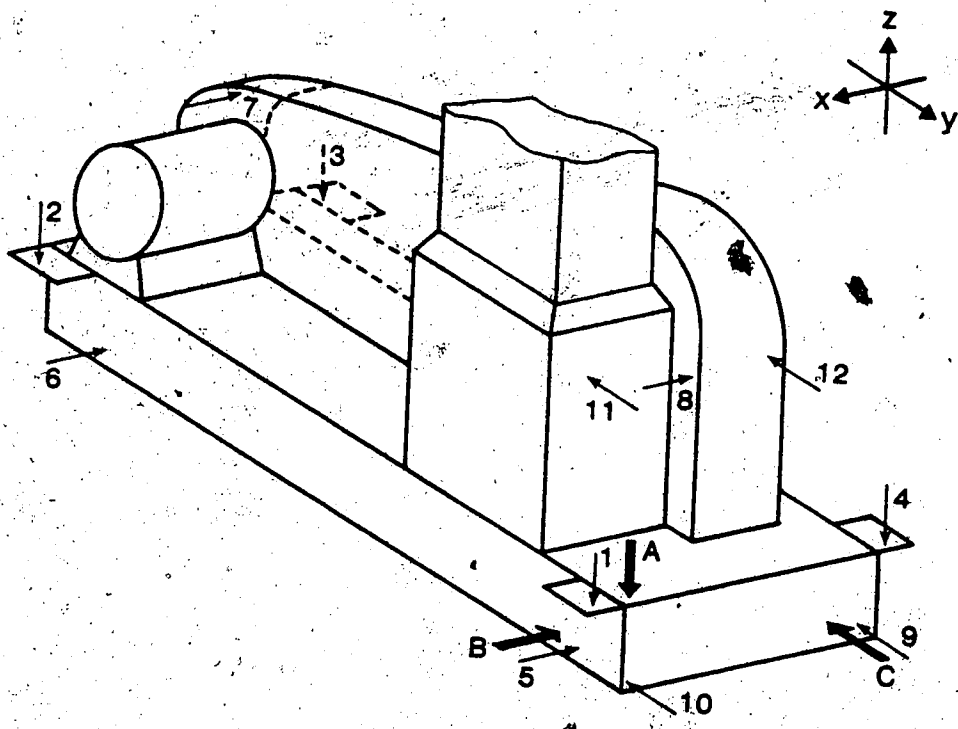


Figure 5.5 Test Points on Compressor System

indicate the impact locations while the other arrows show the points where the response was measured. The test locations were chosen as far apart as possible to give a better definition of the mode shapes and yet in a symmetric manner to simplify the analysis.

In the study of the free-free beam, the accelerometer had been held fixed and the hammer moved from point to point. Due to the layout of the compressor base system however, it was chosen to have a fixed forcing point in each testing plane. This was done because the large hammer used, made it difficult to ensure good clean impacts unless the location was easily accessible and had a flat solid surface (i.e. it was desired to hit the surface squarely and not damage any of the structure in the testing).

Preliminary tests on the structure determined that all of the modes of interest were below 10 Hz. The hammer that was to be used however had a much broader excitation range; the softest head available for the hammer excited a flat frequency response to about 100 Hz. When this signal was recorded on tape and later low pass filtered below 10 Hz for digitizing, very little of the signal was left to work with. To avoid the low signal to noise ratio associated with this, it was decided first to further amplify the impulse signal, then low-pass filter it before recording to maintain as high a signal to noise ratio as possible. In implementing this procedure, some of the inherent advantages and flexibility of this type of recording system were lost, (i.e. it would

be necessary to do further testing if higher frequency analysis ranges were desired) but it was felt that this trade-off was necessary.

The following three figures show examples of transfer functions obtained from testing in each of the three planes. Four distinct modes are present in Figure 5.6 which were obtained by loading the base at point 'A' (in figure 5.5) and recording the response right beside it (point #1). The rounded broad nature of the peaks would indicate that heavy damping was present in the system.

The transfer function formed from forcing the base at point 'B' and picking up the response at point #5 is shown in figure 5.7. In this diagram, five major peaks are seen between the frequency range of 3 Hz and 6.5 Hz. (It was in this range that all six rigid body modes were found.) It should be noted that three peaks located at 3 Hz, 4.7 Hz and 5.4 Hz are common between this figure and figure 5.6.

Shown in figure 5.8 is the transfer function derived from forcing the structure at point 'C' and recording the response at point #10. Two modes are located near 3.1 Hz (as was the case in Figure 5.7) as well as two other modes around 6.2 Hz. The presence of two distinct higher frequency modes is not obvious in the magnitude plot of the transfer function; the phase angle of the function must be studied to see that indeed two separate modes exist in this region.

The modal parameters were then obtained for the six modes by curve fitting the measured transfer functions. The

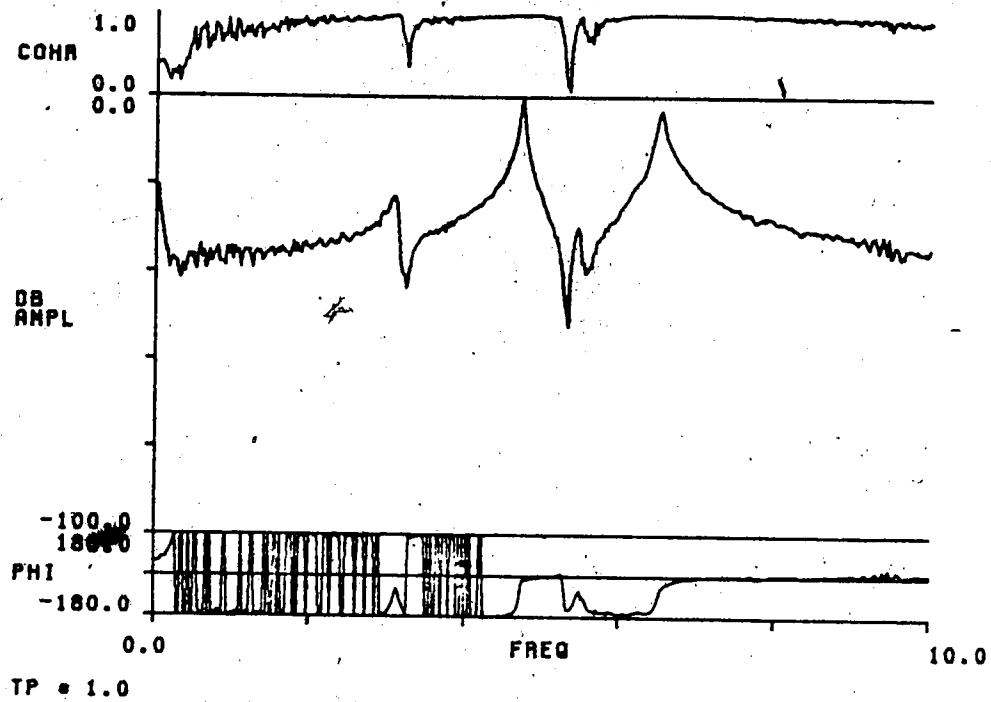


Figure 5.6 Transfer Function in X-Y Plane

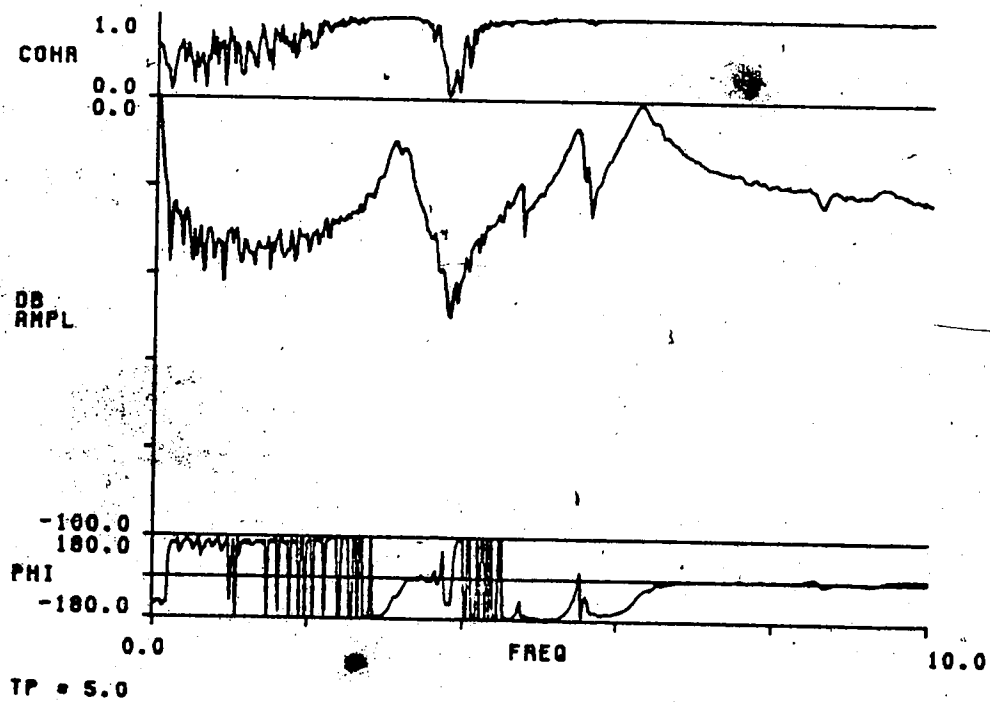


Figure 5.7 Transfer Function in Y-Z Plane

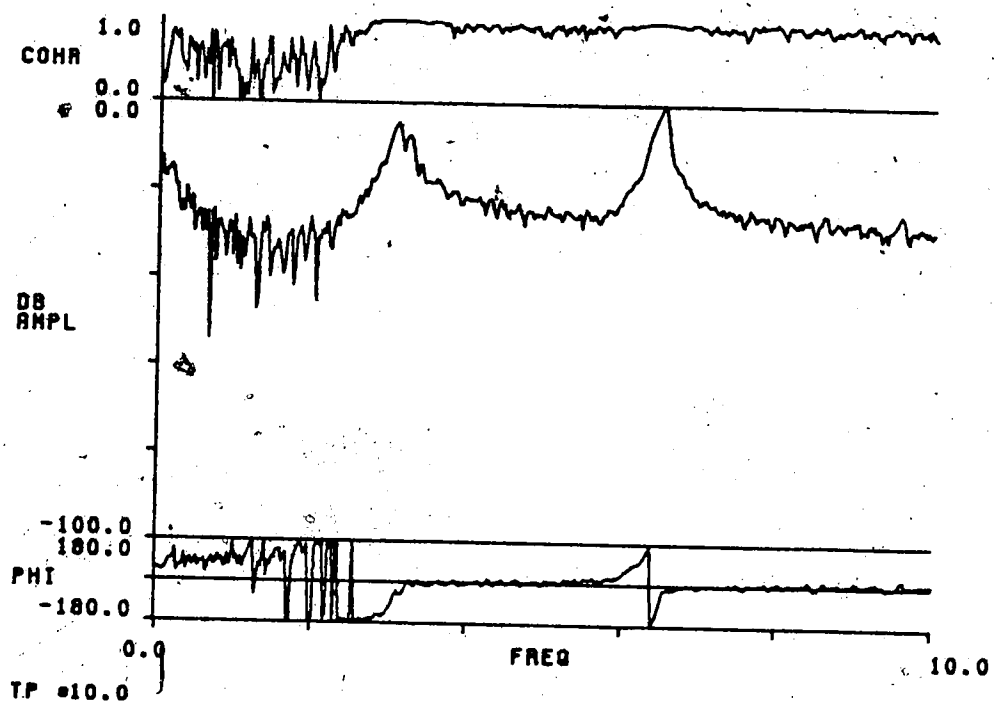


Figure 5.8 Transfer Function in X-Z Plane

tightly spaced modes near 3 Hz and also those around 6.2 Hz caused inconsistencies when curve fitting because of the poor resolution and high overlap of the two modes in either region. This was further hampered by the exponential window (which increases the apparent damping) that was used on the response data to help reduce the noise in the results. (It should be noted that the damping in the system was very heavy; the response signal decayed completely in about one-quarter of the time window, leaving the majority of the signal with a high noise content.)

Table 5.3 lists the averaged resonant frequencies and damping ratios that were obtained from the curve fit of the rigid body modes. The large damping ratios obtained, illustrate the heavy damping that was present in the system.

Shown in figure 5.9 is the mode shape that occurred at a resonant frequency of 6.51 Hz (only the base of the system is shown to simplify the representation of the mode). This mode shape displayed an almost purely rotational mode about the x-axis. The mode shape that was associated with the 6.30 Hz mode is shown in figure 5.10. This was mainly a rotational mode about the z-axis with some light coupling from other modes (especially the rotational mode about the y-axis).

The mode shape associated with the 5.44 Hz resonance was unreliable because of problems associated with curve fitting. What was clear from the results however, was that its major component was that due to rotational motion about

MODE	DAMPING RATIO (%)	RESONANT FREQUENCY (Hz)
1	1.53	3.06
2	0.80	3.22
3	0.25	4.72
4	1.30	5.44
5	1.50	6.30
6	0.55	6.51

Table 5.3 Resonant Frequencies and Damping Ratios of the Compressor System

a line parallel to the y-axis. This behavior is illustrated in Figure 5.11. More coupling from other modes was probably present than what is depicted in this diagram because this rotational motion was also seen in the 6.30 Hz, 4.72 Hz and 3.06 Hz modes. The reasoning behind this is that coupling with the other modes would have been necessary if the effect of this particular motion was viewed in other modes as well (i.e. if two modes are coupled, the effect is seen in both resulting mode shapes).

The mode shape of the 4.72 Hz peak is shown in figure 5.12. This mode consists mainly of a vertical translation with some coupling from the 5.44 Hz mode to produce the small rotation about the y-axis.

Thus far, the modes that have been defined have included three mode shapes that were primarily rotational in nature as well as a fourth mode that had a mainly vertical translation motion. Of the six expected rigid body modes,

this leaves only the two horizontal translation modes to be identified. The mode shapes determined for the resonant frequencies of 3.06 Hz and 3.22 Hz are shown in figures 5.13 and 5.14 respectively (note - the close proximity and heavy damping of the two modes produced inconsistent modal parameters, so that the mode shapes shown are estimates only). Both mode shapes primarily displayed a translational motion with the 3.06 Hz mode translating mainly in the 'y' direction, while the 3.22 Hz mode had the largest component of its displacement in the 'x' direction. If the mass distribution and lateral spring stiffness of the structure had been perfectly symmetric, it could be shown that two purely translational modes with identical natural frequencies would exist. These modes would exhibit physically perpendicular mode shapes with no preferred orientation of movement. When either the spring stiffnesses or the center of mass location, is non-symmetric however, the two frequencies become distinguishable from one another, the modes have a fixed orientation and the mode shapes no longer exhibit perpendicular motion. Therefore in examining the results for the two translational modes, it is not surprising to find that their resonant frequencies are so close together or that their mode shapes show some motion in both the 'x' and 'y' directions.

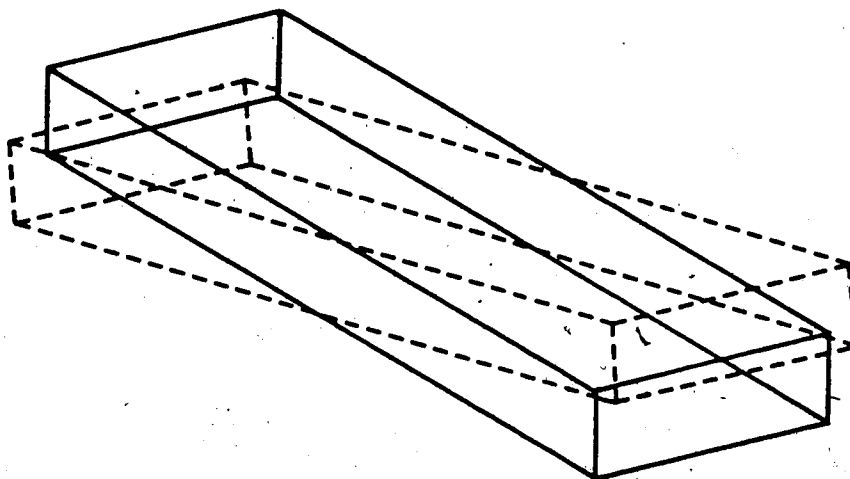


Figure 5.9 Mode Shape of the 6.51 Hz Mode

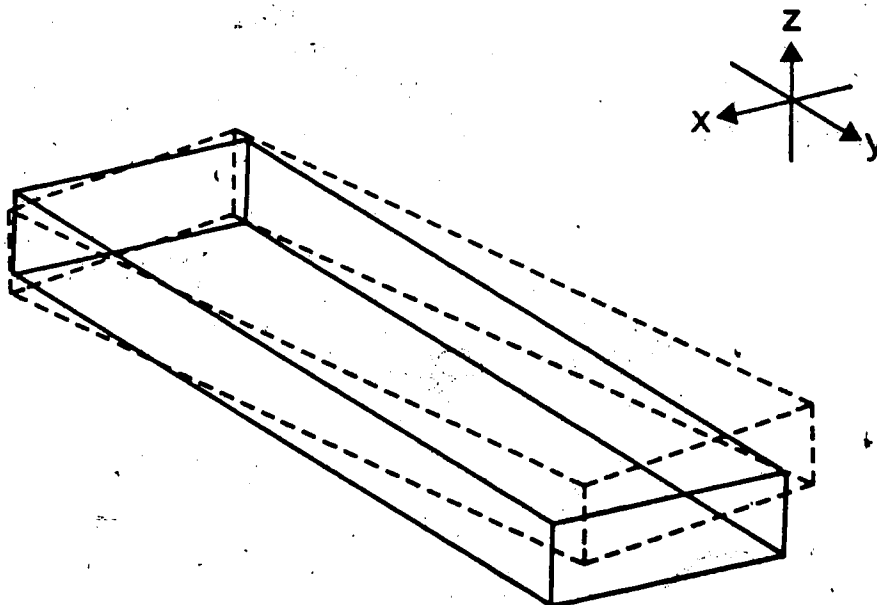


Figure 5.10 Mode Shape of the 6.30 Hz Mode

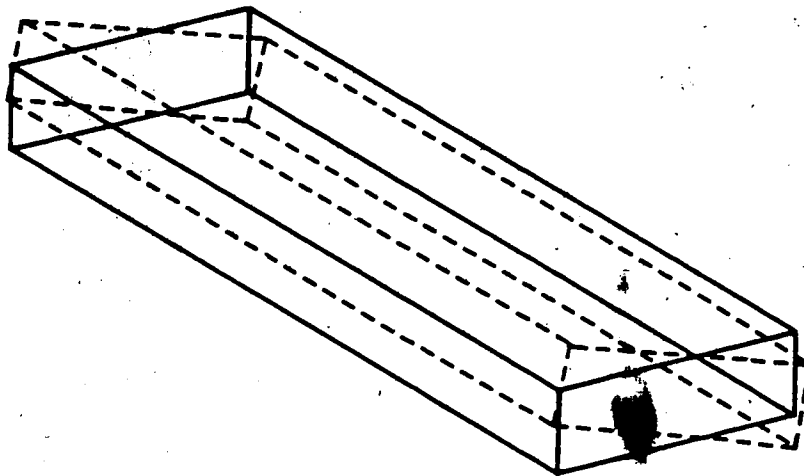


Figure 5.11 Mode Shape of the 5.44 Hz Mode

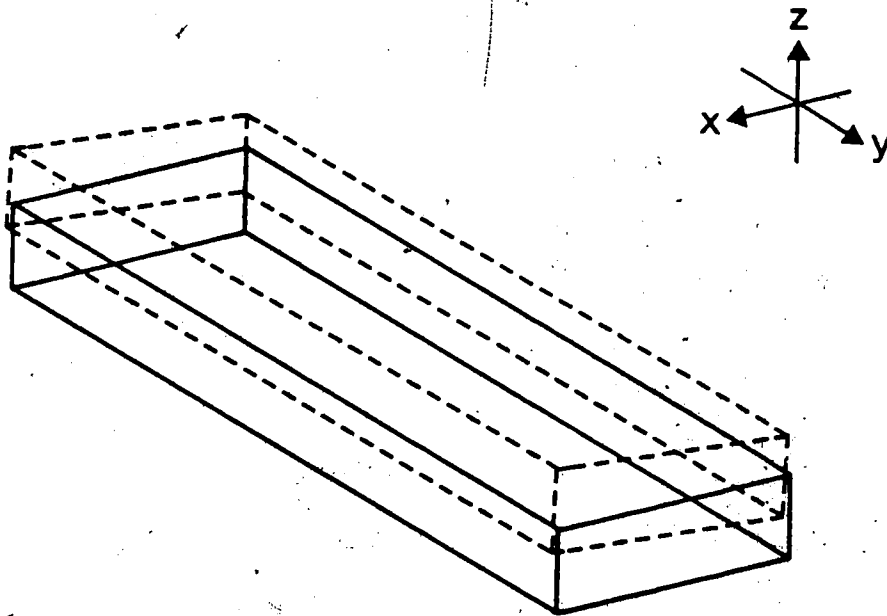


Figure 5.12 Mode Shape of the 4.72 Hz Mode

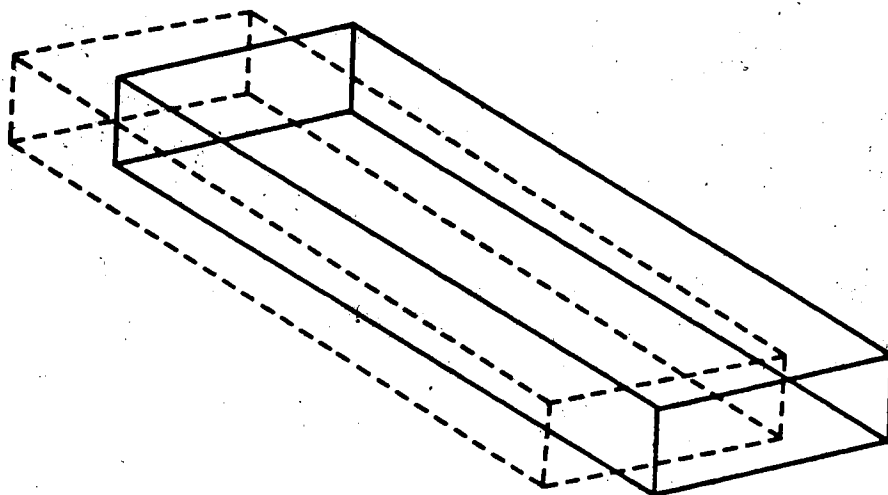


Figure 5.13 Mode Shape of the 3.22 Hz Mode

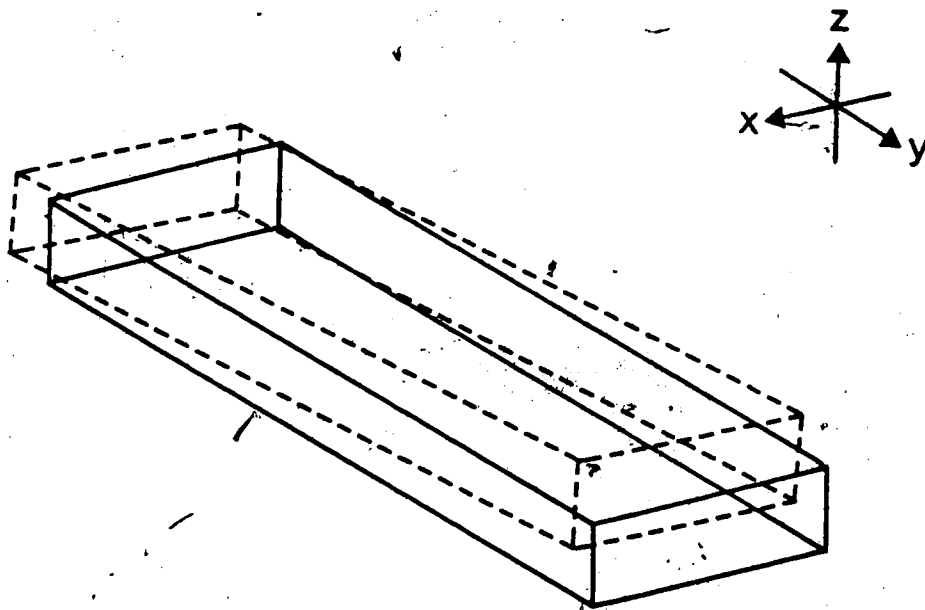


Figure 5.14 Mode Shape of the 3.06 Hz Mode

6. CONCLUSIONS

The testing and analysis regime that has been presented in this study has focused on the practical implementation of the modal analysis technique. Developed during the course of this study was an economical data acquisition system and analysis software that could be readily adapted by smaller engineering firms that could not justify the expense of a sporadically used all-in-one instrumentation system.

From the work done in the study, two things are clear: the first is that good reliable transfer function data can be recorded using commonly available instrumentation. (In fact, the use of a portable tape recorder may be deemed essential in testing locations where on site digitization of the signals is impractical). The second thing to be noted is that modal analysis is not a 'blind' technique that may be effectively applied with little prior knowledge about the method. Familiarity with this type of testing is essential in taking good field measurements and later properly interpreting the derived modal parameters.

The modal parameters identified from the transfer functions of the free-free beam were consistent and reliable. However in dealing with the compressor system, many problems associated with parameter identification were encountered. For the most part, the difficulties could be attributed to the close spacing of some of the modes and the heavy damping in the system. Despite this, it was still possible to separate and identify the modes in question.

However if greater accuracy and more consistent results were desired, it would be necessary to first of all excite the structure in such a way that more energy was being concentrated in the lower frequency range and also to employ 'zoom' Fourier transform techniques to allow greater frequency resolution in the range of interest.

In the course of the study, the area that required the most research time was that involved in curve fitting. The iterative Levy approach that was used in the initial analysis of the transfer functions proved to be very reliable in obtaining preliminary parameter estimates. When further curve fitting was necessary to reduce the errors between the experimental and analytical functions, a good, quick method was not found. Further study in this area would be necessary to research and develop software appropriate for smaller computing facilities.

The next logical stage of development of this modal analysis testing system would be to make use of the modal parameters derived from curve fitting to define a lumped parameter model for the structure being studied (by calculating the mass, damping and stiffness matrices of the system). This would then enable the possibility of using structural modification techniques to quickly determine the effects of any proposed changes to the structure. This type of analysis would be useful in the retro-fitting of existing structures.

REFERENCES

1. Allemang, R.J., "Investigation of Some Multiple Input/Output Frequency Response Function Experimental Modal Analysis Techniques", Ph.D. Dissertation, University of Cincinnati, Mechanical Engineering Department; 1980
2. Bendat, J.S. and Piersol, A.G., *Engineering Applications of Correlation and Spectral Analysis*, John Wiley and Sons; 1980
3. Brigham, E.O., *The Fast Fourier Transform*, Prentice-Hall, Inc., Englewood Cliffs, New Jersey; 1974
4. Brown, D.L., Allemang, R.J., Zimmerman, R. and Mergeay, M., "Parameter Estimation Techniques for Modal Analysis", SAE paper #790221, 19 pp.; 1979
5. Caughey, T.K., "Classical Normal Modes in a Damped Linear Dynamic System", *Journal of Applied Mechanics*; June 1960
6. Doebelin, E.O., *System Modeling and Response*, John Wiley and Sons; 1980
7. Halvorsen, W.G., and Brown, D.L., "Impulse Technique for Structural Frequency Response Testing", *Sound and Vibration*, pp. 8-21; November 1977
8. Irwin, J.D. and Graf, E.R., *Industrial Noise and Vibration Control*, Prentice-Hall, Inc., Englewood Cliffs, New Jersey, pp. 335-351; 1979
9. Kennedy, C.C., and Pancer, C.D.P., "Use of Vectors in Vibration Measurement and Analysis", *J. Aerospace Science*, Vol. 14, No. 11, pp. 603-625; 1947
10. Levy, E.C., "Complex Curve Fitting", *IRE Transactions on Automatic Control*, Vol. AC-4, pp. 37-44; May 1959
11. MacDuff, J.N. and Curreri, J.R., *Vibration Control*, McGraw-Hill Book Company, Inc.; 1958
12. McKinnery, W.H., "Band Selectable Fourier Analysis", *Hewlett-Packard Journal*, pp. 20-24; April 1975
13. Potter, R., "A General Theory of Modal Analysis for Linear Systems", *Shock and Vibration Digest*; November 1975

14. Potter, R. and Richardson, N., "Mass, Stiffness and Damping Matrices from Measured Modal Parameters", I.S.A. Conference and Exhibit, New York City; October 1974
15. Ramsey, K.A., "Effective Measurements for Structural Dynamics Testing-Part ", Sound and Vibration, Vol. 10, No. 4; 1976
16. Ramsey, K.A., "Effective Measurements for Structural Dynamics Testing-Part 1", Sound and Vibration, vol. 9, No. 11; 1975
17. Richardson, M., "Modal Analysis Using Digital Test Systems", Seminar on Understanding Digital Control and Analysis in Vibration Test Systems, Shock and Vibration Information Center Publication, pp. 43-64; May 1975
18. Richardson, M., and Kniskern, J., "Identifying Modes of Large Structures from Multiple Input and Response Measurements", SAE paper #760875 12 pp; 1976
19. Richardson, M. and Potter, R., "Identification of the Modal Properties of an Elastic Structure from Measured Transfer Function Data", Twentieth International Instrumentation Symposium, Albuquerque, New Mexico; May 21-23, 1974
20. Sanathanan, C.K. and Keorner, J., "Transfer Function Synthesis as a Ratio of Two Complex Polynomials", IEEE Transactions on Automatic Control, pp. 56-58; January 1963
21. Walgrave, S.C. and Ehlbeck, J.M., "Understanding Modal Analysis", SAE paper #780695, 11 pp.; 1978
22. "The Fundamentals of Signal Analysis", Hewlett Packard Application Note No. 243

APPENDIX A - LEVY PROGRAM

```

C
C SUBROUTINE LEVY(HEXP,FREQ,NLOW,NHIGH,K,VALUE)
C
C ... COMPUTES A LEAST-SQUARES FIT FOR A TRANSFER FUNCTION
C OF UP TO FIVE MODES USING LEVY'S METHOD
C
C ... HEXP,FREQ - EXPERIMENTAL COMPLEX TRANSFER FUNCTION
C AND CORRESPONDING FREQUENCY LOCATION
C ... NLOW,NHIGH - LOWER AND UPPER LIMIT OF CURVE FIT RANGE
C ... K - NUMBER OF POINTS TO BE FIT IN THE RANGE
C ... VALUE - OUTPUT MODAL PARAMETER VECTOR
C
C ... NOTE : CALCULATIONS WERE DONE IN DOUBLE PRECISION
C BECAUSE 'C' MATRIX WAS FREQUENTLY
C POORLY CONDITIONED
C
REAL*8 C(20,20)/400*0.0D0/,D(20)/20*0.0D0/,WKAREA(500)
REAL*8 RE(401),IM(401),SUM(401),VALUE(20),TWOPI,FF
REAL*8 ABSDEN(401)/401*1.0D0/,TEST,B1,B2,F(21,401)
REAL*8 L(10)/10*0.0D0/,T(10)/10*0.0D0/,S(10)/10*0.0D0/
REAL*8 U(10)/10*0.0D0/,A(11),FREQ*4(401)
COMPLEX*16 Z(10),DEN,ALPHA(10),AA,BB,HEXP*8(401)
COMPLEX*16 ZOLD(10)/10*(0.0D0,0.0D0)/
TWOPI=2.0D0*3.141592653589793
K2=K*2
K4=K*4
K4P1=K4+1
C
C ... PUT POWERS OF FREQUENCY INTO MATRIX F(I,J)
C
DO 100 J=NLOW,NHIGH
F(2,J)=FREQ(J)
RE(J)=REAL(HEXP(J))
IM(J)=AIMAG(HEXP(J))
IF(DABS(F(2,J)).LT.0.0000001) F(2,J)=0.0000001
F(2,J)=F(2,J)*TWOPI
IF(K.GE.3) F(2,J)=F(2,J)/1000.0D0
SUM(J)=RE(J)*RE(J)+IM(J)*IM(J)
DO 100 I=1,K4P1
F(I,J)=F(2,J)**(I-1)
100 CONTINUE
IC=0
GO TO 104
C
C ... CORRECTING FACTORS FOR REDUCING WEIGHTING EFFECTS
C
101 DO 103 J=NLOW,NHIGH
AA=DCMPLX(0.0D0,F(2,J))
DEN=DCMPLX(1.0D0,0.0D0)
DO 102 I=1,K
DEN=DEN+D(K2+I*2-1)*AA**(I*2-1)+D(K2+I*2)*AA**(I*2)
102 CONTINUE

```

```

      ABSDEN(J)=DEN*DCONJG(DEN)
103 CONTINUE
C
C ... COMPUTE CONSTANTS THAT GO INTO 'C' AND 'D' (CX=D)
C
104 DO 105 J=1,K2
      L(J)=0.0D0
      T(J)=0.0D0
      S(J)=0.0D0
      U(J)=0.0D0
105 CONTINUE
      DO 106 I=1,K2
        DO 106 J=NLOW,NHIGH
          L(I)=L(I)+F(2*I-1,J)/ABSDEN(J)
          T(I)=T(I)+F(2*I,J)*IM(J)/ABSDEN(J)
          S(I)=S(I)+F(2*I-1,J)*RE(J)/ABSDEN(J)
          U(I)=U(I)+F(2*I+1,J)*SUM(J)/ABSDEN(J)
106 CONTINUE
C
C ... ELEMENTS IN THE VECTOR 'D'
C
      DO 107 I=1,K
        D(2*I-1)=S(I)
        D(2*I)=T(I)
        D(2*(K+I)-1)=0.0D0
        D(2*(K+I))=U(I)
107 CONTINUE
C
C ... ELEMENTS IN THE MATRIX 'C'
C
      DO 108 J=1,K
        NEG=(-1)**(J+1)
        DO 108 I=1,K
          I2=I*2
          J21=I2-1
          IJ=I+J
          IJ1=IJ-1
          C(I21,J21)=L(IJ1)*NEG
          C(K2+I21,J21)=T(IJ1)*NEG
          C(K2+I2,J21)=S(IJ)*NEG
          C(I2,J2)=L(IJ)*NEG
          C(K2+I21,J2)=S(IJ)*(-NEG)
          C(K2+I2,J2)=T(IJ)*NEG
          C(I21,K2+J21)=T(IJ1)*NEG
          C(I2,K2+J21)=S(IJ)*(-NEG)
          C(K2+I21,K2+J21)=U(IJ1)*NEG
          C(I21,K2+J2)=S(IJ)*NEG
          C(I2,K2+J2)=T(IJ)*NEG
          C(K2+I2,K2+J2)=U(IJ)*NEG
108 CONTINUE
C
C ... CALCULATE 'X', THE SOLUTION VECTOR

```

```

C
    J1=1
    J20=20
    J0=0
C
C ... THE 'IMSL' SUBROUTINE 'LEQT2F' SOLVES A SYSTEM OF
C ... SIMULTANEOUS EQUATIONS
C
    CALL LEQT2F(C,J1,K4,J20,D,J0,WKAREA,IER)
C
C ... DETERMINE THE ZEROES OF THE DENOMINATOR
C
    DO 109 I=1,K2
    A(I)=D(K4P1-I)
109 CONTINUE
    A(K2+1)=1.0D0
C
C ... THE 'IMSL' SUBROUTINE 'ZRPOLY' COMPUTES THE ZEROES
C ... OF A POLYNOMIAL
C
    CALL ZRPOLY(A,K2,Z,IER)
C
C ... CHECK RELATIVE ERROR OF DAMPING AND NATURAL FREQUENCY
C
    TEST=0.0D0
    DO 110 I=2,K2,2
    BB=Z(I)-ZOLD(I)
    B1=DREAL(Z(I))
    B2=DIMAG(Z(I))
    TEST=TEST+DABS(DREAL(BB)/B1)+DABS(DIMAG(BB)/B2)
    ZOLD(I)=Z(I)
110 CONTINUE
    IC=IC+1
    IF(IC.EQ.20) GO TO 111
    IF(TEST/DFLOAT(K2).GT.0.001D0) GO TO 101
    GO TO 113
111 WRITE(10,112)
112 FORMAT(1X,'LEVY DIDN'T CONVERGE IN 20 ITERATIONS')
C
C ... COMPUTE COMPLEX RESIDUES
C
113 DO 115 I=1,K2
    ALPHA(I)=0.0D0
    DO 114 J=1,K
    J2=J*2
    ALPHA(I)=ALPHA(I)+D(J2-1)*Z(I)**(J2-2)+
    #D(J2)*Z(I)**(J2-1)
114 CONTINUE
    ALPHA(I)=ALPHA(I)/D(K4)
    DO 115 J=1,K2
    IF(J.NE.I) ALPHA(I)=ALPHA(I)/(Z(I)-Z(J))
115 CONTINUE
C
C ... CONVERT MODAL PARAMETERS

```


C

```
DO 116 I=1,K
  II=2*I-1
  VALUE(4*I-3)=DIMAG(Z(II))/TWOPI
  VALUE(4*I-2)=DREAL(Z(II))
  VALUE(4*I-1)=DREAL(ALPHA(II))
  VALUE(4*I)=DIMAG(ALPHA(II))
116 CONTINUE
  IF(K.LT.3) GO TO 118
  DO 117 I=1,K4
  VALUE(I)=VALUE(I)*1000.0D0
117 CONTINUE
118 RETURN
END
```

APPENDIX B - NON-SIMULTANEOUS SAMPLING

When using dual or multichannel digitizers, it is often assumed that all of the channels are being digitized simultaneously. This is usually not the case however. Most A/D converters have some finite time lag between the sampling of one channel to the sampling of the second and ensuing channels. If this time lag, t_0 , is very small compared to the sampling period, Δt , (ie. $t_0/\Delta t \rightarrow 0$) the data collected will be valid. As the digitizing speed is increased (t_0 is fixed), the relationship between the signals on two separate channels will become noticeably different from two which are simultaneously sampled. The time-shifting property of the Fourier transform pair can be used to examine this effect.

Consider a signal $h(t)$ and its Fourier transform $H(f)$. If $h(t)$ is shifted along the 't' axis by an amount t_0 , it can be shown that the Fourier transform of this function, $h(t-t_0)$ is $H(f)\exp(-j\omega t_0)$. To get the desired frequency spectrum, $H(f)$, that would have occurred had the sampling been truly simultaneous ($t_0=0$), it is necessary to simply divide the calculated Fourier transform by the factor $\exp(-j\omega t_0)$. If the product ωt_0 (which is proportional to $t_0/\Delta t$) is small, then this factor approaches the value of one (real valued only). Thus small sampling delays cause little distortion to the spectrum of interest. However, if the term ωt_0 , has some appreciable value, then the factor $\exp(-j\omega t_0)$ will be complex valued and will affect the phase

angle of the spectrum (the magnitude stays the same).

In practical testing then, it is necessary to determine what time delay (if any) is present between the channels of the digitizer. If the ratio $t_0/\Delta t$ is small, it may be chosen to neglect the correction term (typically if t_0 is less than 1% of Δt , the correction is ignored). Generally however, the addition of the correction factor can be simply implemented into the analysis procedure, so that any time delays can be corrected.